

## REVIEW SUMMARY

## 2D MATERIALS

# Graphene, related two-dimensional crystals, and hybrid systems for energy conversion and storage

Francesco Bonaccorso,\* Luigi Colombo, Guihua Yu, Meryl Stoller, Valentina Tozzini, Andrea C. Ferrari, Rodney S. Ruoff, Vittorio Pellegrini

**BACKGROUND:** The integration of graphene in photovoltaic modules, fuel cells, batteries, supercapacitors, and devices for hydrogen generation offers opportunities to tackle challenges driven by the increasing global energy demand. Graphene's two-dimensional (2D) nature leads to a theoretical surface-to-mass ratio of  $\sim 2600 \text{ m}^2/\text{g}$ , which combined with its high electrical conductivity and flexibility, gives it the potential to store electric charge, ions, or hydrogen. Other 2D crystals, such as transition metal chalcogenides (TMDs) and transition metal oxides, are also promising and are now gaining increasing attention for en-

ergy applications. The advantage of using such 2D crystals is linked to the possibility of creating and designing layered artificial structures with "on-demand" properties by means of spin-on processes, or layer-by-layer assembly. This approach exploits the availability of materials with metallic, semiconducting, and insulating properties.

**ADVANCES:** The success of graphene and related materials (GRMs) for energy applications crucially depends on the development and optimization of production methods. High-volume liquid-phase exfoliation is being

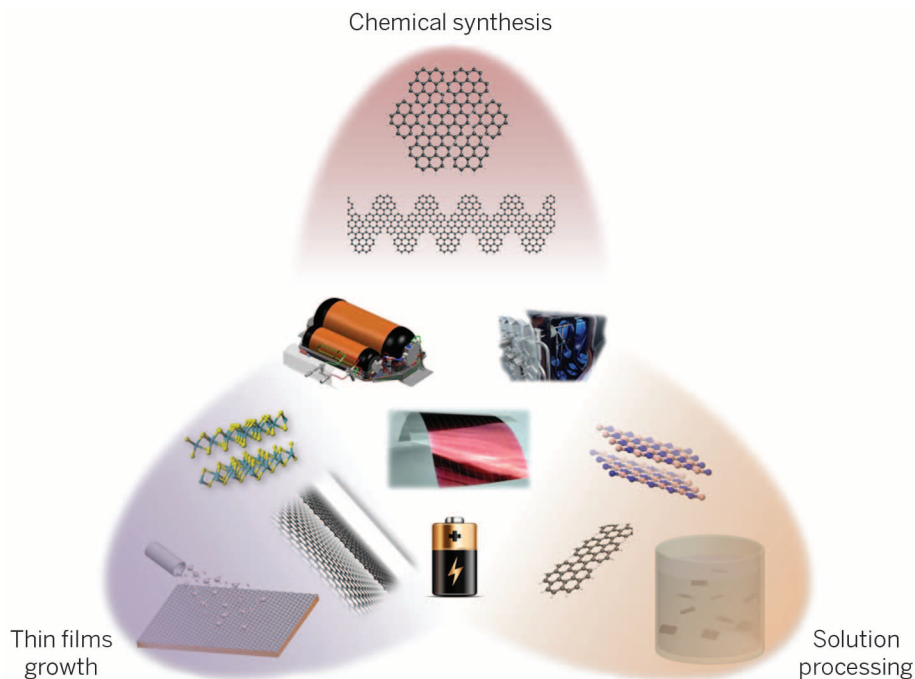
developed for a wide variety of layered materials. This technique is being optimized to control the flake size and to increase the edge-to-surface ratio, which is crucial for optimizing electrode performance in fuel cells and batteries. Micro- or nanocrystal or flake edge control can also be achieved through chemical synthesis. This is an ideal route for functionalization, in order to improve storage capacity. Large-area growth via chemical vapor deposition (CVD) has been demonstrated, producing material with high structural and electronic quality for the preparation of transparent conducting electrodes

## ON OUR WEB SITE

Read the full article at <http://dx.doi.org/10.1126/science.1246501>

for displays and touchscreens, and is being evaluated for photovoltaic applications. CVD growth of other multicomponent layered materials is less mature and needs further development. Although many transfer techniques have been developed successfully, further improvement of high-volume manufacturing and transfer processes for multilayered heterostructures is needed. In this context, layer-by-layer assembly may enable the realization of devices with on-demand properties for targeted applications, such as photovoltaic devices in which photon absorption in TMDs is combined with charge transport in graphene.

**OUTLOOK:** Substantial progress has been made on the preparation of GRMs at the laboratory level. However, cost-effective production of GRMs on an industrial scale is needed to create the future energy value chain. Applications that could benefit the most from GRMs include flexible electronics, batteries with efficient anodes and cathodes, supercapacitors with high energy density, and solar cells. The realization of GRMs with specific transport and insulating properties on demand is an important goal. Additional energy applications of GRMs comprise water splitting and hydrogen production. As an example, the edges of  $\text{MoS}_2$  single layers can oxidize fuels—such as hydrogen, methanol, and ethanol—in fuel cells, and GRM membranes can be used in fuel cells to improve proton exchange. Functionalized graphene can be exploited for water splitting and hydrogen production. Flexible and wearable devices and membranes incorporating GRMs can also generate electricity from motion, as well as from water and gas flows. ■



**GRMs for energy applications.** The ability to produce GRMs with desired specific properties paves the way to their integration in a variety of energy devices. Solution processing and chemical vapor deposition are the ideal means to produce thin films that can be used as electrodes in energy devices (such as solar panels, batteries, fuel cells, or in hydrogen storage). Chemical synthesis is an attractive route to produce "active" elements in solar cells or thermoelectric devices.

The list of author affiliations is available in the full article online.  
\*Corresponding author. E-mail: francesco.bonaccorso@iit.it  
Cite this article as F. Bonaccorso et al., *Science* 347, 1246501 (2015). DOI: 10.1126/science.1246501

## REVIEW

## 2D MATERIALS

# Graphene, related two-dimensional crystals, and hybrid systems for energy conversion and storage

Francesco Bonaccorso,<sup>1,2\*</sup> Luigi Colombo,<sup>3</sup> Guihua Yu,<sup>4</sup> Meryl Stoller,<sup>5</sup> Valentina Tozzini,<sup>6</sup> Andrea C. Ferrari,<sup>2</sup> Rodney S. Ruoff,<sup>7</sup> Vittorio Pellegrini<sup>1,6</sup>

Graphene and related two-dimensional crystals and hybrid systems showcase several key properties that can address emerging energy needs, in particular for the ever growing market of portable and wearable energy conversion and storage devices. Graphene's flexibility, large surface area, and chemical stability, combined with its excellent electrical and thermal conductivity, make it promising as a catalyst in fuel and dye-sensitized solar cells. Chemically functionalized graphene can also improve storage and diffusion of ionic species and electric charge in batteries and supercapacitors. Two-dimensional crystals provide optoelectronic and photocatalytic properties complementing those of graphene, enabling the realization of ultrathin-film photovoltaic devices or systems for hydrogen production. Here, we review the use of graphene and related materials for energy conversion and storage, outlining the roadmap for future applications.

The development of reliable and environmentally friendly approaches for energy conversion and storage is one of the key challenges that our society is facing. Wearable energy conversion and storage devices require flexible, lightweight, conductive materials with a large surface-to-mass ratio [specific surface area (SSA)(m<sup>2</sup>/g)] to allow storing and releasing of "particles" (such as lithium ions, hydrogen atoms or molecules, or electric charges).

A sheet of graphene has a theoretical SSA = 2630 m<sup>2</sup>/g (1). This is much larger than that reported to date for carbon black [typically smaller than 900 m<sup>2</sup>/g (2)] or for carbon nanotubes (CNTs), from ≈100 to 1000 m<sup>2</sup>/g (1), and is similar to activated carbon (carbon processed with oxygen to make it porous) (3). The large SSA of graphene—when combined with its high electrical conductivity (4), high mechanical strength (5), ease of functionalization (6), and potential for mass production (7)—makes it an ideal platform for energy applications, such as a transparent conductive electrode for solar cells or as flexible high-capacity electrode in lithium-ion batteries and supercapacitors. Moreover, the combination of chem-

ical functionalization and curvature control opens new opportunities for hydrogen storage (8, 9).

Other two-dimensional (2D) crystals, such as the transition metal dichalcogenides (TMDs) (for example, WS<sub>2</sub>, MoS<sub>2</sub>, and WSe<sub>2</sub>), display insulating, semiconducting (with band gaps in the visible region of the spectrum), and metallic behavior and can enable novel device architectures also in combination with graphene (10). As for the case of graphene, these materials can be integrated on flexible surfaces and can be mass-produced. Another class of 2D crystals is the MXenes (11, 12), derived by exfoliating the so-called MAX phases: layered, hexagonal carbides and nitrides that can accommodate various ions and molecules between their layers by intercalation (11, 12). MXene sheets are promising for energy applications, such as lithium-ion batteries (11), supercapacitors (12), and hydrogen storage (13).

Some 2D crystals are also promising for fuel cells and in water-splitting applications because of the large photocatalytic properties of their edges (14). The creation of hybrids with graphene and other nanomaterials, such as CNTs, can find applications in energy storage devices, such as supercapacitors (15), but also in photovoltaics. For simplicity, we will refer to graphene and related materials (GRMs) (16).

The challenge is to develop GRMs with properties tailored to create new devices that can be assembled for large-scale energy conversion (photovoltaics, thermoelectric, or fuel cells), and storage (supercapacitors, batteries, or hydrogen storage). This will require the production of high-quality material in high volumes by means of liquid-phase exfoliation (LPE)—for example, via ultrasonication (7, 17) or shear mixing (18). Large-

area GRMs grown by means of chemical vapor deposition can also play a role because they can have better morphological and optical/electric properties than those of LPE materials. Chemical synthesis (19) is also a possible route to tailor the shape of graphene flakes with atomic precision, but the scale-up remains challenging (7). A review of GRMs production is provided in (7).

## Energy conversion in solar cells, thermoelectric devices, and fuel cells

In a photovoltaic (PV) device or solar cell, the incoming radiation creates electron-hole pairs in the active material. These are then separated and transported to electrodes [for example, Fig. 1A refers to a dye-sensitized solar cell (DSSC)] (20). Because graphene does not have a band gap and absorbs 2.3% of the incoming radiation almost independent of wavelength (21), it can capture a much broader spectrum than can semiconductors used today [for comparison, a silicon layer with the same thickness as graphene would absorb ~0.03% of the incident radiation at a wavelength of 500 nm (22)]. Graphene can perform different functions in inorganic and organic solar cells, such as transparent conductive electrodes (23, 24) and counter-electrodes (25–27). Other layered materials (LMs) with a band gap in the visible region of the electromagnetic spectrum [(such as MoS<sub>2</sub> (Fig. 1B)] and chemically functionalized graphene can be used as photosensitizers, which transform absorbed photons into electrons (20). Graphene quantum dots (28) or graphene nanoribbons (GNRs) also enable a higher optical absorption close to their band gap (28).

In a thermoelectric device, a potential difference between electron and hole-doped crystals is created by a temperature gradient, as shown in Fig. 1C. GNRs or graphene with engineered defects can potentially improve the conversion efficiency (the ratio between the energy provided to the external load and the thermal energy absorbed) with respect to conventional thermoelectric materials based on PbTe or Bi<sub>2</sub>Te<sub>3</sub> and their alloys (29), in addition to decreasing the environmental impact and cost.

Last, fuel cell devices in which electrical energy is generated by the conversion of chemical energy via redox reactions at the anode and cathode (Fig. 1D) (30, 31), can also take advantage of GRMs as catalysts, so as to replace more expensive noble metals, such as platinum (30), with the added value of enabling more flexible and lighter devices.

## Solar cells

The key figures of merit of solar cells are (32) the internal photocurrent efficiency, or the fraction of absorbed photons converted into electrical current; the external quantum efficiency, or the fraction of incident photons converted into electrical current; and the energy conversion efficiency  $\eta = P_{\text{max}}/P_{\text{inc}}$ , where  $P_{\text{inc}}$  is the incident power and  $P_{\text{max}} = V_{\text{OC}} \times I_{\text{SC}} \times FF$ , where  $V_{\text{OC}}$  is the maximum open-circuit voltage,  $I_{\text{SC}}$  is the maximum short-circuit current, and  $FF$  is the fill factor, defined as  $(V_{\text{max}} \times I_{\text{max}})/(V_{\text{OC}} \times I_{\text{SC}})$ , with  $V_{\text{max}}$  and  $I_{\text{max}}$  the maximum voltage and current, respectively (32).

<sup>1</sup>Istituto Italiano di Tecnologia, Graphene Labs, Via Morego 30, I-16163 Genova, Italy. <sup>2</sup>Cambridge Graphene Centre, University of Cambridge, Cambridge CB3 0FA, UK. <sup>3</sup>Texas Instruments, Dallas, TX 75243, USA. <sup>4</sup>Materials Science and Engineering Program and Department of Mechanical Engineering, University of Texas at Austin, Austin, TX 78712-0292, USA. <sup>5</sup>nCarbon, Austin, TX 78727, USA. <sup>6</sup>National Enterprise for nanoScience and nanoTechnology, Istituto Nanoscienze-CNR and Scuola Normale Superiore, I-56126 Pisa, Italy. <sup>7</sup>Center for Multidimensional Carbon Materials, Institute for Basic Science, Department of Chemistry, Ulsan National Institute of Science & Technology, UNIST-gil 50, Eonyang-eup, Ulsu-gun, Ulsan 689-798, Republic of Korea. \*Corresponding author. E-mail: francesco.bonaccorso@iit.it

Silicon is the most widely used absorber to date (20) and currently dominates the PV device market. State-of-the-art silicon-PV devices based on p-n junctions, often referred to as first-generation solar cells (20), have an efficiency of up to ~25% (32). The development of second-generation PVs, based on thin-film technologies, has been driven by the need to increase efficiency (32). However, to date the efficiency of second-generation PVs is below that of silicon (32). Third-generation PVs rely on the exploitation of emerging organic PV cells (33), DSSCs (Fig. 1A) (34), and quantum dots solar cells (QDSCs) (35), which may be less expensive, more versatile, and perhaps more environmentally friendly (34). However, they have lower efficiency [~12 and ~13% for organic PV cells (36) and DSSCs (27), respectively], low stability, and lower strength as compared with those of first- and second-generation PV cells. An important recent development is the meso-super-structured solar cell (37), based on an organic halide perovskite LMs (such as  $\text{CH}_3\text{NH}_3\text{PbX}_3$ , where X is chlorine, bromine iodine, or their combination) as photosensitizer (37, 38), and an organic hole-transport material (38). An efficiency of 15.6% in a meso-super-structured (perovskite) solar cell for an un-optimized device was reported in (38), whereas an efficiency of 20.1% has been recently developed at KRICT (Korean Research Institute of Chemical Technology) (39). However, these LMs may not satisfy sustainability requirements because of their lead content.

Driven by the need for new “environmentally friendly” materials, that can further improve efficiency and/or reduce cost of photovoltaic devices, GRMs are being developed as transparent conductors (TCs) (23, 24, 40), photosensitizers (10, 28), channels for charge transport (41, 42), and catalysts (25, 43). The use of GRMs for TCs to replace indium tin oxide (ITO), and catalysts to replace platinum, can improve the performance/cost ratio. For example, the use of graphene nanoplatelets as electro-catalysts for the polypyridine complexes of Co(III)/(II) in DSSCs allowed the achievement of the new record of efficiency of 13% (27) (Fig. 1A). The replacement of platinum, which is routinely used as an electro-catalyst in DSSCs, with GRMs may result in almost four orders of magnitude cost reduction. (The costs are based on Sigma-Aldrich values available at [www.sigmaaldrich.com](http://www.sigmaaldrich.com).)

#### Transparent conductive window

Transparent conducting films can act both as windows to the photosensitizer and as an ohmic contact (32). The key requirements for transparent conductive windows in PV systems are low sheet resistance [ $R_s < 10$  ohms per square (44)] and high transmittance (Tr) [ $> 90\%$  (44)].  $R_s$  has units of ohms, as resistance does, but it is historically quoted in “ohms per square,” which is defined as  $R = R_s \times L/W$ , where  $L/W$  is defined as the number of squares of side  $W$  that can be superimposed on the resistor without overlapping (21). The search for previously unidentified and less expensive conductive materials with good chemical stability, high Tr, and high electric

conductivity is crucial for cost reduction. Today, the conductive support [such as ITO, or fluorine-doped tin oxide (FTO)] is one of the most expensive component of a DSSC (45). Beyond cost, the need for flexibility limits the use of current TC substrates. ITO and FTO are usually deposited at temperatures higher than the thermal stability of the polymeric substrates; additionally, their brittleness makes it difficult to use them when flexibility is a requirement (21).

Although the combined  $R_s$  and Tr targets have not been achieved yet, graphene-based TC windows were implemented in a variety of solar cell systems: inorganic (46), organic (23), DSSCs (40), and hybrid organic/inorganic (24). Given the continued progress in both quality [such as growth of graphene single crystals  $> 1$  cm (47)] and scalability [such as development of roll-to-roll (48) production lines], graphene-based TCs are an appealing alternative to ITO and FTO (21).  $R_s \sim 30$  ohms per square and Tr  $\sim 90\%$  were achieved via doping (49). TCs based on graphene doped with bis(trifluoromethanesulfonyl)-amide [( $\text{CF}_3\text{SO}_2$ ) $_2\text{NH}$ ] resulted in graphene/n-silicon Schottky junction solar cells with a  $\eta = 8.6\%$  (50), whereas TCs based on graphene doped with nitric acid used in an organic/silicon cell yielded  $\eta \sim 10.34\%$  (24). Hybrid structures, such as graphene/

metal grids (51), have also been considered. Graphene/metal grids were reported with  $R_s = 20$  ohms per square and Tr = 90% (51). Transparent conductive windows based on other LMs (such as  $\text{Bi}_2\text{Se}_3$ ) have been fabricated on mica with  $R_s = 330$  ohms per square and Tr = 70% (52), which is still well below state-of-the-art graphene-based TCs (49, 51). More work, however, is needed for a conclusive assessment on their applicability as TCs.

#### Photosensitizers

The key requirements of a photosensitizer depend on the type of solar cell. In general, an efficient sensitizer should have the ability to absorb light over a wide energy range (32–34), high carrier mobility (32), and thermal and photochemical stability (33, 34). There are other more specific requirements for the various types of solar cells regarding, for example, the charge separation between donor/acceptor materials in organic PVs (33) and the efficiency of electronic injection from the photosensitizer into the  $\text{TiO}_2$  in DSSCs (34).

Transition metal coordination compounds such as ruthenium complexes (53) and synthetic organic dyes (54) are used as sensitizers in DSSCs. However, the preparation routes for

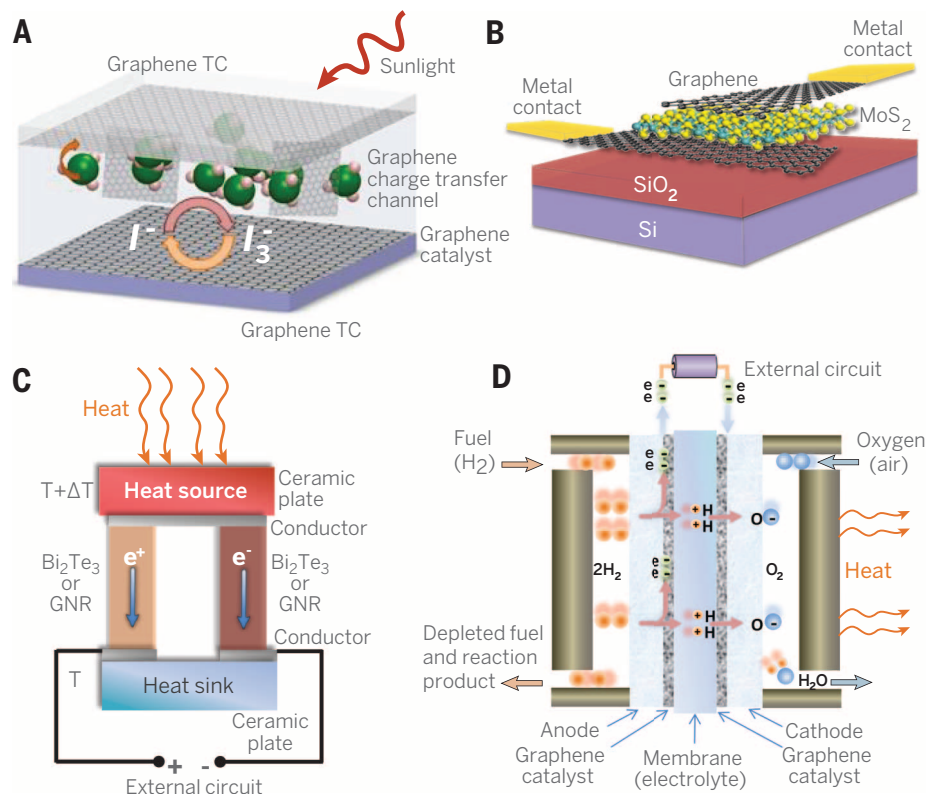


**Fig. 1. Energy conversion devices.** (A) Schematic of a dye-sensitized solar cell (DSSC) with graphene used in several components, as detailed in the text. (B) Heterostructure (graphene/ $\text{MoS}_2$ /graphene) photovoltaic device. (C) Schematic illustration of power generation in a thermoelectric device based on LM  $\text{Bi}_2\text{Te}_3$  or GNRs. A temperature gradient,  $\Delta T$ , causes charge carriers in the material to diffuse, resulting in current flow through the external circuit. (D) Proton exchange membrane fuel cells (31). Fuel (for example,  $\text{H}_2$ ) channeled from one side of the cell is split by the catalyst (a GRM electrode) into  $\text{H}^+$  ions and  $\text{e}^-$ . Electrons generate a current in the external circuit and then combine with  $\text{H}^+$  and the oxidant ( $\text{O}_2$ ) at the cathode, forming water and heat.

metal complexes are multi-step, involving long and expensive chromatographic purification, whereas organic dyes have a narrow spectral absorption and low electric conductivity. GRMs, on the other hand, have superior optoelectronic properties (21), which can be tuned by means of chemical synthesis (19, 28) or post-production functionalization (55).

Chemically functionalized graphene (with organic molecules, conjugated polymers, rare-earth components, and inorganic semiconductors) (55), chemically synthesized GNRs (56), and quantum dots (28) have been used as photosensitizers (28, 55). However, although graphene quantum dots have molar extinction coefficient [absorbance of light per unit path length (in centimeters) and per unit of concentration (moles per liter)] of  $\sim 1 \times 10^5 \text{ M}^{-1} \text{ cm}^{-1}$  (28), which is about one order of magnitude larger than inorganic dyes (such as ruthenium complexes) (28), the energy conversion efficiency is still too low as a consequence of low current density ( $200 \mu\text{A}/\text{cm}^2$ ) (28). This is due to low chemical affinity between the graphene quantum dots and the  $\text{TiO}_2$  surface, resulting in poor charge injection (28). Calculations based on equivalent electric circuits for organic PVs (56) indicate that  $\eta \sim 12\%$ , which is comparable with the state-of-the-art organic PVs (36), could be achieved with GNR photosensitizers (56).

TMDs are also potential photosensitizers (Fig. 1B) because of their large optical absorption [up to 10% or more of the incident light in a thickness of less than 1 nm (57), when in resonance], band gaps in the visible region, and chemical stability. For example, graphene/ $\text{WS}_2$  vertical hybrid structures were studied for PV applications, with  $\text{WS}_2$  acting as a photosensitizer (10). The van Hove singularities in the electronic density of states of  $\text{WS}_2$  allowed large photon absorption and electron-hole creation with an external quantum efficiency (the ratio of the number of charge carriers collected by the solar cell to the number of photons) of  $\sim 33\%$ . An alternative route is to combine metal nanoparticles with graphene, a method that can increase its light-harvesting capacity by more than one order of magnitude (58), making this hybrid structure a candidate photosensitizer.

#### Channel for charge transport

Charge-collection and transport are other important issues in PV devices. The transport of photo-generated electrons across the  $\text{TiO}_2$  nanoparticle network (34) in DSSCs competes with charge recombination (34), a major bottleneck for increasing efficiency. In order to suppress charge recombination and increase photo-generated carriers, 1D materials such as CNTs can be used, but the cost and 1D nature (limiting the point contact between  $\text{TiO}_2$  nanoparticles and CNTs) call for a better alternative. Graphene, with its high electron mobility (4), could be integrated with  $\text{TiO}_2$  films to enhance the electron transfer properties of the photoanode.

Reduced graphene oxide [RGO (7), or rGO (59)], was incorporated into nanostructured  $\text{TiO}_2$  (41) and ZnO (42) photo-anodes in DSSCs in or-

der to enhance the charge transport rate by preventing charge carrier recombination. RGO allows the use of thicker photo-anodes (42) [higher dye loading and consequently higher light harvesting (34)], thus improving efficiency with respect to conventional DSSCs (41). An energy conversion efficiency  $\eta = 5.86\%$  was reported in (42) for a DSSC composed of a 9- $\mu\text{m}$ -thick ZnO photo-anode with 1.2 weight % RGO loading, which is higher than DSSCs with “conventional” photo-anodes of the same thickness (41).

The electron collection layer is also important in perovskite solar cells (37), in which high-temperature sintered n-type  $\text{TiO}_2$  electron-selective contacts are used (38), but this increases the cost and hinders the use of plastic substrates (38). Replacing the sintered  $\text{TiO}_2$  should make perovskite solar cells a more versatile technology for inorganic PVs. Few-layers graphene (FLG) flakes, prepared via solution processing and incorporated in  $\text{TiO}_2$  nanoparticles, were used as electron collection layer in perovskite-based solar cells (60), achieving  $\eta \sim 15.6\%$  owing to the superior charge-collection of the FLG- $\text{TiO}_2$  composite, with respect to bare  $\text{TiO}_2$  ( $\eta = 10\%$ ) (60). This  $\eta$  matches perovskite solar cells (38) and is the highest among graphene-based solar cells reported to date (Fig. 2).

Charge transport and collection also have a fundamental role in organic PVs (OPV). For example, in a poly-3-hexyl thiophene (P3HT)/phenyl-C61-butyric acid methyl ester (PCBM) solar cell, both the donor (P3HT) and acceptor (PCBM) materials are in direct electrical contact with the cathode (back electrode) and anode (ITO) electrodes, leading to carrier recombination (61). To reduce such a negative effect, electron blocking and hole transport layers are usually deposited on top of ITO (61). Currently, the most popular

hole transport layers are wide-band gap p-type materials, such as NiO,  $\text{MoO}_3$ ,  $\text{V}_2\text{O}_5$ , and poly(3,4-ethylenedioxythiophene) poly(styrenesulfonate) (PEDOT:PSS) (33, 61). However, inorganic hole transport layers are deposited by vacuum techniques, incompatible with the roll-to-roll processes used in OPV, whereas PEDOT:PSS is usually deposited from highly acidic ( $\text{pH} = 1$ ) aqueous dispersions (61). These corrode the ITO and can also introduce water into the active layer (processed in organic solvents), thus degrading device performance (61).

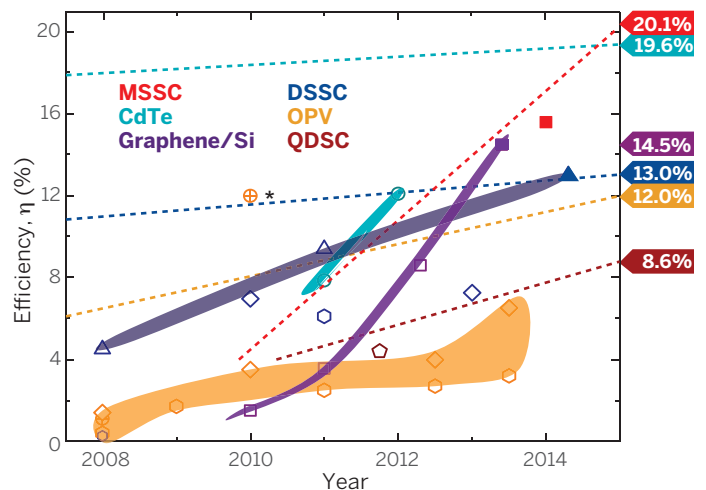
GRMs have been used as hole transport layers in OPV (61–63). OPV devices based on GO as the hole transport layer have shown  $\eta = 3.5\%$ , which is comparable with devices fabricated with PEDOT:PSS ( $\eta = 3.6\%$ ) (61), whereas OPV exploiting RGO as hole transport layers were reported with  $\eta = 3.98\%$ , which is superior to PEDOT:PSS ( $\eta = 3.6\%$ ) (62). Graphene quantum dots can also be efficient hole transport layers for OPVs, with  $\eta = 6.82\%$  (63), showing longer lifetime and more reproducible performance with respect to PEDOT:PSS-based cells (63).

#### Counter-electrode

The role of the counter-electrode in a DSSC is twofold: It (i) back-transfers electrons arriving from the external circuit to the redox system and (ii) catalyzes the reduction of the charge mediator (34). The key requirements for counter-electrodes are high exchange current density (the rate of electron transfer between electrolyte and electrode), low charge-transfer resistance (the electrode-electrolyte interface resistance), and high SSA (59). Currently, DSSC counter-electrodes are made of platinum layers, which are expensive, deposited onto conductive electrodes, ITO or FTO (34). Moreover, platinum tends to degrade over

**Fig. 2. Solar energy conversion efficiency of GRM-based photovoltaic devices.**

Colors define different classes of GRM-based photovoltaic devices: purple, graphene/silicon (46, 50, 68); orange, organic photovoltaics (OPVs) (23, 24, 56); dark blue, DSSCs (25, 41–43); light blue, CdTe (67); dark red, QDSCs (35); light red, meso-structured solar cells (MSSCs) (60). Symbols are linked to different functions of the GRMs for each photovoltaic device: hexagons (23, 24), transparent conductor; triangles (25–27), counter-electrode; rhombuses (41, 42), charge transport. Orange closed areas cluster different GRM functions in OPVs. The data on the right axis refer to state-of-the-art PV efficiency (32), with the dashed lines representing the performance timeline of devices based on non-GRM materials [data taken from (32)]. The asterisk close to the crossed circle refers to a theoretical work for graphene nanoribbons as a photosensitizer in OPVs (56).



time when in contact with the tri-Iodide/Iodide ( $I_3^-/I^-$ ) liquid electrolyte, reducing the efficiency. Thus, the replacement of such elements with lower cost and/or more reliable materials (leading to high-efficiency devices) is needed. Graphene can satisfy all the counter-electrode requirements because of its high SSA (59), which is essential to help the  $I_3^-$  reduction, high electric conductivity (4), low charge-transfer resistance (25), and lower cost than platinum.

Graphene oxide (43) and hybrid structures of RGO-CNTs (64) have been used as counter electrodes in DSSCs, with results close to the state of the art with platinum (Fig. 2). Graphene nanoplatelets (sheets of functionalized graphene with an overall thickness ranging from ~2 to ~15 nm) are now emerging as the best performing counter-electrodes in DSSCs, with (27) reporting the highest  $\eta$  to date of 13%.

The need to develop a platinum-free counter-electrode has seen a rising interest also in inorganic LMs such as transition metal oxide (TMO) and metal carbides, nitrides, and sulfides (65). Thin flakes of  $MoS_2$  and  $WS_2$  counter-electrodes were used in (65), with the  $I_3^-/I^-$  redox couple, achieving  $\eta = 7.59$  and 7.73%, respectively, which is close to that of platinum counter-electrodes. In particular, platinum was outperformed as a counter-electrode by  $MoS_2$  (4.97%) and  $WS_2$  (5.24%) in DSSCs using an organic disulfide/thiolate ( $T_2/T^-$ ) redox couple (65). Hybrid systems, such as graphene- $MoS_2$ , were also used as counter-electrodes in DSSCs, achieving  $\eta = 5.81\%$  (66). Thus, although to date  $\eta$  is lower than the best reported for platinum (12.3%) and graphene nanoplatelets (13%) (27), with further optimization 2D crystals (65) and hybrids (66) could play a key role as counter-electrodes in DSSCs.

### Outlook

GRMs exploited as counter-electrodes in DSSCs (65, 66) or in CdTe (67) solar cells show encouraging results. The efficiency of PV devices based on GRMs is progressing at a pace superior to those based on conventional materials (32). The highest  $\eta = 13\%$  to date for DSSCs was recently achieved by using graphene nanoplatelets as a counter-electrode. Graphene/silicon hybrid solar cells, although first reported in 2010 (46), already have  $\eta = 14.5\%$  (68), whereas graphene-based perovskite solar cells have  $\eta = 15.6\%$  (60) for low-temperature (<150°C) processing, matching that reported for high-temperature (>500°C) cells (38), thus with an advantage in processing and cost reduction. In Fig. 2, we compare  $\eta$  of GRM and conventional non-GRM-based PV devices. The results to date could enable integration in existing devices with higher  $\eta$  and the development of new-concept devices, such as graphene/silicon solar cells.

### Thermoelectric devices

About half of the energy generated worldwide is lost as waste heat (69, 70). Thermoelectrics, solid-state devices (Fig. 1C) that generate electricity from a temperature gradient, are ideal to recover waste thermal energy (69, 70). Thermoelectric

devices can also convert heat produced by concentrated or unconcentrated sunlight, into electricity (69, 70). This is important because infrared radiation with photon energies below the band gap of the photosensitizers is not absorbed in conventional PV cells and generates only waste heat (69, 70).

In a typical thermoelectric device, a junction is formed between two different n- and p-doped conducting materials (Fig. 1C). A heat source at the junction causes carriers to flow away from it, resulting in a “thermo-electric” generator (exploiting the Seebeck effect, resulting in a voltage induced by a temperature gradient). In a thermoelectric device, many of these junctions are connected electrically in series and thermally in parallel. They can also work inversely, using electricity to generate or remove heat. When a current is passed in the appropriate direction through a junction, both types of charge carriers move from the junction and transport heat away, thus cooling the junction (Peltier effect). Thermoelectric devices are appealing, but their low efficiencies limit their widespread use.

The effectiveness of a thermoelectric device is assessed in two ways: by its Carnot efficiency (the fraction of absorbed heat that is converted into work) and by a material-dependent figure of merit, known as  $zT$ ;  $zT = TS^2\sigma/k$  (69), where  $S$  is the Seebeck coefficient,  $T$  is the temperature,  $\sigma$  is the electric conductivity,  $\kappa$  is the thermal conductivity, and  $z = S^2\sigma/k$  (69). Thus, thermoelectric materials require high  $S$  and  $\sigma$  and low  $\kappa$  (69). In order to optimize  $zT$ , phonons must experience a high scattering rate, thus lowering thermal conductivity [like in a glass (69, 70)], whereas electrons must experience very little scattering, maintaining high electric conductivity (as in a crystal) (70).

The majority of explored materials in thermoelectric devices have  $zT \sim 1$  (69). LMs such as  $Bi_2Te_3$ , PbTe, and their alloys (29) and, in par-

ticular, the  $(Bi_{1-x}Sb_x)_2(Se_{1-y}Te_y)_3$  alloy family have been in commercial use for several decades because of their room-temperature  $zT \sim 1$  and Carnot conversion efficiencies ~5 to 6% (69). State-of-the-art thermoelectric materials design relies on engineering of the scattering mechanisms for phonons (70) and charge carriers (70). Currently, superlattices of  $Bi_2Te_3/Sb_2Te_3$  (71) and quantum dots fabricated by means of atomic layer deposition designed to disrupt the phonon mean free path, while still allowing good electron mobilities, have the highest  $zT \sim 2.4$  to 2.9 at 300 to 400 K (71) and 3.5 at 575 K, respectively (72).

Graphene has both high electric (4) and thermal (73) conductivity, a combination not ideal for thermoelectric devices. However, it is possible to tailor the thermal transport properties of graphene by nano-structuring techniques, such as defect (74) and isotope (75) engineering or edge roughness (74), or by introducing periodic nano-holes (76). The combination of geometrical structuring, GNRs with predefined geometries (19), and isotopic enrichment with  $^{13}C$  (75) can reduce thermal conductivity by up to two orders of magnitude with respect to pristine graphene (77). It has been estimated that  $zT$  up to 3.25 can be achieved by exploiting GNRs that have a chevron-like geometry (77). However, scaling up of GNRs via chemical synthesis (19) still poses a challenge. Nevertheless, the modulation of geometric factors determining electric and thermal conductivity might be achieved via LPE. This technique also allows the blending of LMs with CNTs in order to increase the electrical conductivity while not reducing the Seebeck coefficient.

Advances in nanostructuring (74–76) to create hybrid structures on demand, with high electrical conductivity and low thermal conductivity, could accelerate the development of high-performance GRMs for thermoelectric devices.

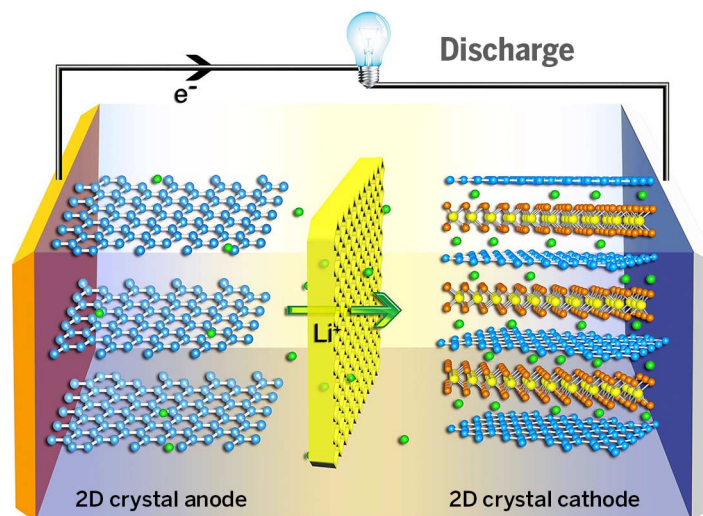


**Fig. 3. Schematic of GRMs-based battery electrodes.** In this example, the anode is composed of graphene flakes, but other 2D crystals can also be used, alone or in hybrid structures, as detailed in the text. The cathode is a hybrid graphene-lithium compound (such as  $LiCoO_2$  or  $LiFePO_4$ ), designed to enhance electron transport kinetics compared with graphene-free lithium compounds.

## Fuel cells

Fuel cells convert chemical energy from a fuel into electricity via a reaction with oxygen or other oxidizing agents (Fig. 1D) (31). Their development goes hand-by-hand with hydrogen production and storage. In the next section, we will outline the use of GRMs for production and storage of hydrogen. Here, we focus on the possible use of GRMs in conversion of hydrogen into electrical energy in fuel cells.

The integration of fuel cells in electronics faces several challenges: (i) electrodes suitable for flexible electronics; (ii) replacement of expensive noble metals such as platinum, ruthenium, gold, and their alloys as electro-catalysts; and (iii) the need to avoid metal electrode poisoning (31). To address these challenges, a new class of materials with low cost, high efficiency (both for fuel oxidation at the anode and oxygen reduction reaction at the cathode), and durability have to be developed before fuel cells can be considered as a serious technology for energy conversion in electronic devices. GRMs are an ideal material platform to address these challenges and facilitate the transport of electrons produced during both fuel oxidation and oxygen reduction reaction (30). Moreover, GRMs have been demonstrated to be attractive candidates as proton membranes owing to their high proton conductivity (78). This, coupled with impermeability to water, H<sub>2</sub>, and methanol, might solve the problem of fuel cross-over and electrode poisoning (78). Several GRMs are being investigated both as alternative to metal catalysts (30) or to be used in conjunction with platinum in hybrid structures (79). As demonstrated in (79), graphene-supported platinum and Pt–Ru nanoparticles have higher methanol and ethanol oxidations in comparison with those of the widely-used Vulcan XC-72R carbon black catalyst. As demonstrated in (80), RGO modifies the properties of platinum electro-catalysts supported on it. Platinum/graphene hybrid electro-catalysts were shown to have a high activity for methanol oxidation compared with commercial platinum/carbon black (80).

GRMs have also shown catalytic properties for oxygen reduction reactions at the cathode. It was reported in (30) that edge-halogenated graphene nanoplatelets, produced via high-volume scalable ball-milling, outperformed commercial platinum catalysts. LMs such as perovskites also have good catalytic activity at the cathode surface in solid-oxide fuel cells, thanks to their mixed ionic-electronic conductivity (81).

The possibility to tune the GRM lateral size and thickness (7), thus increasing their edge/bulk atoms ratio, can improve the catalytic activity because a higher number of active catalytic sites are present at the edges (14) for fuel oxidation at the anode and oxygen reduction at the cathode. This will be a step forward in making GRMs a key set of materials for the development of cheaper and more efficient fuel cells.

## Energy storage

Current energy storage devices are based on the capture and release of lithium ions, electric charges,

or hydrogen atoms or molecules. For example, lithium-ion batteries (82), now ubiquitous in portable electronics, consist of an intercalated lithium compound cathode, a graphitic anode, and an electrolyte. Crucial to the performance of these rechargeable batteries is the gravimetric capacity to store lithium ions (the charge stored per gram of battery weight). Compared with graphite, graphene and other related materials have a larger theoretical gravimetric capacity (83). Additionally, the use of graphene enables flexible and/or stretchable battery devices (84). Similar advantages also apply to electrochemical double-layer capacitors (EDLCs), which are currently formed via electrode/electrolyte systems based on two symmetric activated carbon electrodes impregnated with electrolytes (85). Other relevant properties of GRMs are the electrochemical and thermal stability within the device's operational temperature range (–50 to 100 °C).

## Batteries

Most of the commercial rechargeable lithium-ion batteries are based on a LiCoO<sub>2</sub> cathode and a graphite anode. This combination has a theoretical energy density of 387 Wh kg<sup>–1</sup> (86) and a measured energy density of 120 to ~150 Wh kg<sup>–1</sup> (86), which is higher than that of other batteries, such as lead acid [–30 Wh/kg (87)] and nickel metal hydrides (45 to 68 Wh/kg) (87). Potential oxide host structures, not yet commercialized, include ordered olivine Li<sub>1–x</sub>MPO<sub>4</sub> (M = Fe, Mn, or Ni) (88), layered Li<sub>1–x</sub>MO<sub>2</sub> (M = Ni, Mn, or Co) (89), and spinel LiMn<sub>2</sub>O<sub>4</sub> (90).

GRMs can improve the gravimetric capacity and energy density compared with current technology owing to GRMs' high electrical conductivity (4), high SSA (59), large number of active sites for Li<sup>+</sup> storage, and short Li<sup>+</sup> diffusion distances (91). Indeed, GRMs are appealing both as cathodes (92) and anodes (Fig. 3) (83). Graphene, in particular, has a theoretical specific capacity [total ampere-hours (Ah) available when the battery is discharged at a certain discharge current, per unit weight] of 744 mAh g<sup>–1</sup> assuming lithium adsorbed on both sides of graphene to form Li<sub>2</sub>C<sub>6</sub> (83).

The discharge current is often expressed as a C-rate in order to normalize against battery-specific capacity. The C-rate is a measure of the rate at which a battery is discharged relative to its maximum capacity, hence the name (82). For example, at 1C the battery will discharge in 1 hour. A specific capacity of 540 mAh g<sup>–1</sup> for RGO-based electrodes was reported in (93), and up to 730 and 784 mAh g<sup>–1</sup> in RGO-CNT and RGO-C<sub>60</sub> hybrid systems, respectively. Edges and defects could act as reversible lithium storage sites, thus contributing to the specific capacity (83). The importance of edges for lithium uptake has been demonstrated in (91), in which an anode containing <100-nm LPE flakes, deposited by inks, achieved a specific capacity of ~1500 mAh g<sup>–1</sup> at a discharge current of 100 mA g<sup>–1</sup>. The anode has also shown a specific capacity of 165 mAh g<sup>–1</sup> at 1C when assembled in a full-battery configuration (91). Graphene-based hybrid electrodes (94), in which graphene is used as a substrate for electrochemically active nanoparticles (such as Li<sub>1–x</sub>MPO<sub>4</sub> or

LiMn<sub>1–x</sub>Fe<sub>x</sub>PO<sub>4</sub>) have been exploited to increase electron transport, specific capacity, C-rate, and cyclability (the number of charge/discharge cycles before the battery-specific capacity falls below 60% of the nominal value). Graphene was also used as a substrate for the growth of anode/cathode nanomaterials [for example, olivine-type phosphates (94)] to achieve higher-rate-performance electrodes with respect to nonconducting materials (94). For example, LiMn<sub>1–x</sub>Fe<sub>x</sub>PO<sub>4</sub> nanorods grown on RGO flakes have shown only a 1.9% degradation for 100 cycles of the nominal capacity ~100 mAh g<sup>–1</sup> at 50 C. This improved electrochemical performance, with respect to graphite or RGO, is attributed to Li<sup>+</sup> rapid diffusion along the radial direction of the nanocrystals, in addition to facilitated electron transport between RGO and nanocrystals. A similar approach to create GRMs-based hybrid electrodes was applied to different materials, such as other olivine-type phosphates (95), and spinels (96).

Another pathway to increase the charge/discharge capacity and C-rate of lithium-ion batteries is to confine the electrochemically active particles (such as sulfur, Co<sub>3</sub>O<sub>4</sub>, Fe<sub>3</sub>O<sub>4</sub>, or Li<sub>3</sub>VO<sub>4</sub>) within the graphene flakes (97). For example, in hybrid electrodes, graphene flakes wrapping Co<sub>3</sub>O<sub>4</sub> nanoparticles can suppress nanoparticle aggregation and accommodate their volume expansion/contraction upon lithiation/de-lithiation, in addition to ensuring high electrical conductivity (90). Thus, the specific capacity and cycling performance of hybrid RGO/Fe<sub>3</sub>O<sub>4</sub> (98) or RGO/Li<sub>3</sub>VO<sub>4</sub> (99), for example, improves as compared with electrodes made of nanoparticles alone (98, 99).

The third approach for electrode optimization targets flexible and/or stretchable battery devices (84), which are able to accommodate large strain while retaining their function. GO flakes have been exploited to fabricate a flexible, layer-by-layer assembled conducting scaffold with tolerance to structural deformation (100). Such 3D flexible scaffolds loaded with silicon nanoparticles have shown a specific capacity of 1100 mAh g<sup>–1</sup> at a discharge current of 8 A g<sup>–1</sup>, degrading ~0.34% per cycle for 150 cycles (100).

TMDs, TMOs, and TMHs (transition metal hydroxides) are also promising for batteries (101). Some of the TMDs are accessible for lithium intercalation and exhibit fast ionic conductivity (101). Examples include TiS<sub>2</sub> as an electrochemically active material (102) and exfoliated MoS<sub>2</sub> flakes (103). A ~750mAh g<sup>–1</sup> specific capacity was reported in (103) when using turbostratically restacked MoS<sub>2</sub> single layers as battery electrodes. The restacking enlarges the *c* axis parameter—the space between layers—thus increasing the accessible SSA (103). ZrS<sub>2</sub> colloidal nanodisks with diameters of ~20 nm delivered a specific capacity ~600 mAh g<sup>–1</sup> (104). Hybrid WS<sub>2</sub>/RGO composites were used as electrodes, achieving ~450 mAh g<sup>–1</sup> at 0.1 A g<sup>–1</sup> and ~240 mAh g<sup>–1</sup> at ~4 A g<sup>–1</sup>, respectively (105).

MXenes, such as Ti<sub>2</sub>AlC, have shown lithiation/delithiation peaks at 1.6 and 2 V versus Li<sup>+</sup>/Li (11). At 1C, the specific capacity was 110 mAh g<sup>–1</sup> after 80 cycles. Compared with materials currently

used in lithium and sodium ion battery anodes, MXenes show promise in increasing overall battery performance (11).

### Supercapacitors

Supercapacitors store energy using either ion adsorption (EDLC) (85) or redox reactions (106), in which most of the charge is transferred at or near the surface of the electrode material [pseudocapacitors (106)]. Supercapacitors are ideal for applications in which high power density [at least 10 kW Kg<sup>-1</sup> (85, 106), one order of magnitude larger than lithium-ion batteries] is needed, such as in the case of energy recapture and delivery in hybrid vehicles, mass transit, load cranes, load leveling, and backup power for electric utilities and factories (106).

#### EDLC supercapacitors

Almost all commercial EDLCs are based on two symmetric electrodes impregnated with electrolytes comprising tetraethylammonium tetrafluoroborate salts in organic solvents [acetonitrile (AN) and propylene carbonate (PC)] (85). Current commercial packaged EDLC supercapacitors, with organic electrolytes operating at 2.7 V, reach energy densities ~5 to 8 Wh/kg and 7 to 10 Wh/liter (85). Another type of supercapacitor based on lithium-ion hybrid cells [in which a graphite lithium-ion anode is coupled with an AC supercapacitor cathode (107)] is also offered commercially with energy densities of ~10 to 14 Wh/kg and 18 to 25 Wh/liter (107).

In an EDLC, energy is stored by forming an electrical double layer of electrolyte ions on the surface of conductive electrodes (Fig. 4A) (108). EDLCs are not limited by the electrochemical charge transfer kinetics of batteries and thus can operate at charge/discharge rates of the order of seconds, and with lifetimes of >1 million cycles (106). The EDLC energy density is determined by the square of the operating voltage ( $V_0$ ) and the specific capacitance [capacitance per unit mass (farad per gram) or volume (farad per cubic centimeter)] of the electrode/electrolyte system: Wh/Kg =  $\xi(F/g) \times (V_0)^2$ , where  $\xi$  is a constant (85). The specific capacitance in turn is related to the electrode's SSA accessible by the electrolyte, its interfacial double-layer capacitance (farad per square centimeter), and the electrode material density (109). The need to maintain electrochemical stability limits the operating voltage with organic electrolytes to ~2.7 V (106) because higher voltages result in electrolyte breakdown.

As in the case of batteries, electrode materials for EDLCs must be produced in tons and processed into electrodes 100 to 200  $\mu\text{m}$  thick (109, 110) to be commercially viable. Because the weight of the active electrode material when used as a thin coating is negligible compared with the support material, energy and power densities measured at the active material level do not translate to current commercial EDLC performances when scaled to full-size devices (109, 110). Specific capacitances as high as ~190 F/g (111) in aqueous electrolytes and ~120 F/g in organic electrolytes were obtained with RGO produced by different

routes (112), but all with SSAs <700 m<sup>2</sup>/g, which is far short of the theoretical 2630 m<sup>2</sup>/g (59). One approach to increase the SSA accessible to the electrolyte is the use of graphene-based platelets with spacer materials such as CNTs (15), mesoporous carbon spheres (113), water and ionic liquids (114), and resin that is subsequently chemically activated to create a porous structure (115). The reported SSAs range from 421 (15) to 1810 m<sup>2</sup>/g (115). The activation of microwave expanded graphite oxide with KOH forms a porous material comprised of highly curved single-layer sheets of  $n$ -membered rings of carbon, with  $n$  varying between 5 and 8, and with measured SSA of 3100 m<sup>2</sup>/g (3). Hydrothermal carbonization of either biomass or polymer mixed with dispersed GO, followed by chemical activation, yielded a 3D structure with nanoscale pores and a SSA of 3523 m<sup>2</sup>/g (116). However, although these values are higher than that of graphene, the measured SSA should be considered as an apparent or equivalent area because the Brunauer-Emmett-Teller (BET) method used for the determination of SSA is not applicable to microporous solids (3).

The interfacial capacitance of high-SSA GRMs comprises both the quantum capacitance (the response of the charge to the conduction and valence band movement, proportional to the electronic density of states) and the capacitance of the solid electrolyte interface (107). High SSA alone is, however, not sufficient to further increase performance of EDLC electrodes (107). High SSA and interfacial capacitance do not necessarily translate into high specific capacitance. A low packing density (<0.5 g/cm<sup>3</sup>), for example, leads

to empty space in the electrode that will be flooded by the electrolyte, increasing the cost and weight of the device, without adding capacity (109). Larger densities (~1.58 g/cm<sup>3</sup>) were achieved by evaporation drying of graphene hydrogel, yielding specific capacitances of ~167 F/cm<sup>3</sup> in organic electrolyte (117). Capillary compression of RGO gave electrode densities of ~1.25 g/cm<sup>3</sup> and a specific capacitance of ~206 F/cm<sup>3</sup> in ionic liquids (118). Another method to increase energy storage capacity is to increase the operating voltage. To this end, graphene-based electrodes with ionic liquid electrolytes operating at voltages up to 3.5 V and in a wide temperature range (-50 to 200°C) are currently being investigated (119, 120).

Intercalation of cations (such as Na<sup>+</sup>, K<sup>+</sup>, Mg<sub>2</sub><sup>+</sup>, NH<sub>4</sub><sup>+</sup>, and Al<sub>3</sub><sup>+</sup>) from aqueous salt solutions between Ti<sub>3</sub>C<sub>2</sub> MXene was reported (12). A specific capacitance in excess of 300 F/cm<sup>3</sup>, higher than in porous carbons, was reported in (12).

#### Hybrid and Pseudocapacitors

A different type of supercapacitor contains at least one electrode material with redox reactions that occur close to the electrode surface (pseudocapacitor) or a secondary battery electrode. Lithium-ion hybrid supercapacitors combine the rapid charge/discharge and long cycle life of an EDLC electrode with the higher energy storage capacity of a lithium-ion battery anode (121). However, the higher energy density currently comes with the trade-off of slower charge/discharge rates, lower efficiency, and reduced cycle life. Activated microwave expanded graphite oxide EDLC electrodes with lithium-ion battery electrodes comprising graphite (122), Li<sub>4</sub>T<sub>5</sub>O<sub>12</sub> (122), and Fe<sub>3</sub>O<sub>4</sub>

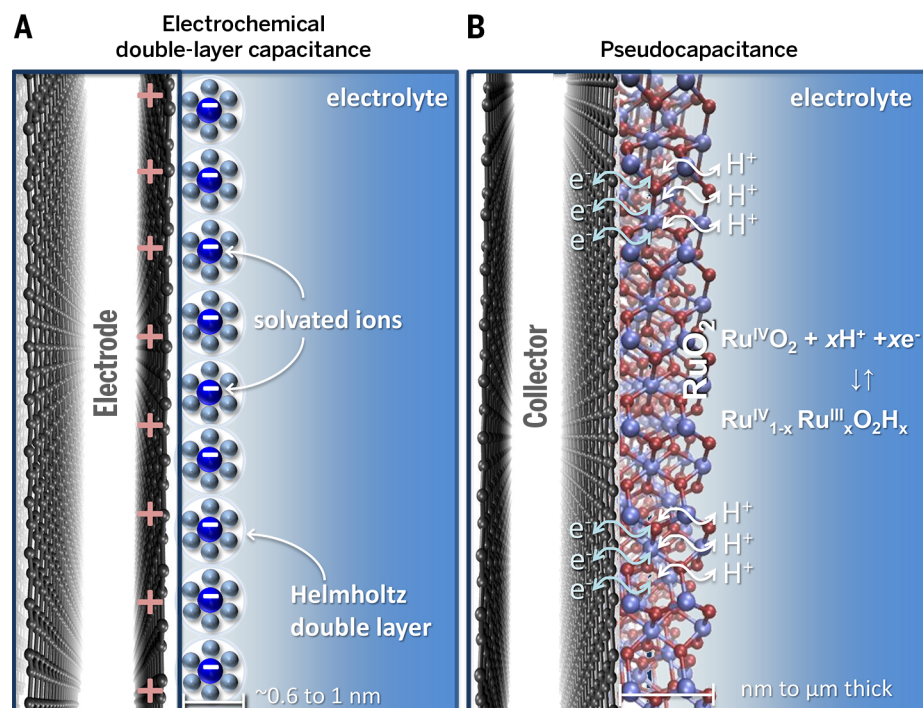


**Fig. 4. Schematic of charge storage in supercapacitors.** (A) Ion adsorption at the electrode surface (EDLC). (B) Charge transfer near the surface of the electrode (pseudocapacitance).

(123) were studied. Also, electrodes containing metal oxides such as  $\text{RuO}_2$ ,  $\text{MnO}_2$ ,  $\text{MoO}_3$  and conducting polymers were used to increase the specific capacitance via redox reactions (Fig. 4B) (108). In these systems, graphene was used as conductive support for composites with  $\text{MnO}_2$  (124) and with conductive polymers such as polyaniline (125).

### Hydrogen production and storage

The chemical energy density of hydrogen is 142 MJ/kg, which is more than three times that of gasoline. The by-product of its combustion is water. Thus, hydrogen is one of the most interesting “green” fuels. GRMs can help address the two main issues related to the use of hydrogen as fuel: (i) production and (ii) storage/transportation.

The key mechanism for the production of hydrogen gas is the hydrogen evolution reaction (HER;  $2\text{H}^+ + \text{e}^- \rightarrow \text{H}_2$ ). The edges of 2D crystals, such as  $\text{MoS}_2$  and  $\text{WS}_2$  (126), and hybrid systems (such as  $\text{MoS}_2/\text{RGO}$ ) (127) are active catalytic sites, making them promising electrodes for the HER (126, 127). However, the HER mechanism varies from material to material (126); thus, its understanding is fundamental for the optimized use of GRMs (126, 128). Resistive losses are one of the key problems for nonmetallic electrodes (31). Thus, combinations of 2D crystals with CNTs (128) and graphene (126) are being explored to further enhance HER by improving the electron transport efficiency.

Storage is also a challenge in hydrogen technology. The approach based on liquefying and pressurizing hydrogen presents safety issues. Solid-state storage is thus being investigated as an alternative.

Carbon-based structures are particularly attractive for hydrogen storage because carbon is a light element, and graphene in particular has potentially the most favorable gravimetric density among the carbon-based materials [the weight percentage of stored hydrogen (Fig. 5)] (129). The storage of molecular hydrogen in graphene relies on the van der Waals forces (binding energy of  $\sim 0.01$  to  $0.06$  eV/molecule (129), leading to theoretical estimates of gravimetric density of  $\sim 3.3\%$  (129), which is increased up to 8% in multi-layers spaced by pillar structures or CNTs (130) at cryogenic temperatures and/or high pressure. The estimated range of gravimetric density at ambient conditions is 1 to 4% (130). Experimental data are lower, in the range of 2 to 6% for low temperature and/or high pressures and  $\sim 1\%$  at ambient conditions (Fig. 5, orange band) (131). Semiconductor LMs, such as InSe and GaSe (132), are reported to have gravimetric densities of up to 3 to 4%, obtained by a combination of electrochemical and thermal treatments (Fig. 5, blue and purple bands). In this case, hydrogen intercalates between the layers (132).

Decorating graphene with alkaline (133) or transition metals (133) can increase the hydrogen adsorption energy, leading to a theoretical gravimetric density up to 10%. Stronger binding is obtained by chemisorption (Fig. 5, gray band) leading to the formation graphane (8, 134). The use of chemisorption as a storage mechanism requires overcoming the high  $\text{H}_2$  chemi(de)sorption barriers [ $\sim 1.5$  eV/atom (8)] to achieve loading/release kinetics at room temperature. Possible catalytic strategies for hydrogen adsorption/desorption involve the functionalization of graphene with metals such as palladium (135), known

to catalyze the dissociation of hydrogen molecules into ions onto the graphene surface, or the combined effect of nitrogen-substitutional doping and an electric field normal to the sheet, which is predicted to produce dissociation-adsorption of  $\text{H}_2$  (136).

The peculiar structural and mechanical properties of graphene enable alternative strategies for adsorption/desorption. It was theoretically (137) and experimentally shown (134) that the hydrogen affinity is enhanced on the convex areas and reduced on the concave areas of rippled graphene. The possibility of controlling load and release by modifying the local curvature was predicted with density functional theory (Fig. 5, structures at top) (8). To this end, mechanisms to control the curvature of graphene should be identified: the use of transverse acoustic phonons generated by a piezoelectric substrate (9) or inducing piezoelectricity within graphene by means of specific doping or decoration (138) were suggested.

### Perspective

Graphene, related 2D crystals, and hybrid systems might play a major role in future energy conversion and storage technologies. The ability to produce these GRMs, and control their properties, might enable a range of device characteristics, with optimized energy/power densities, lifetime, safety, and potentially reducing cost while minimizing environmental impact. To be commercially viable, GRMs must substantially surpass the performance of existing materials at comparable manufacturing costs. For example, GRMs have been reported with specific capacitances of  $\sim 300$  F/cm<sup>2</sup>, which is much higher than chemically activated state-of-the-art carbons. The ability to create stacked hetero-structures of metallic, semiconducting, and insulating 2D crystals might enable an even broader spectrum of device structures, perhaps with tunable properties. This might enable bulk thermoelectric materials with on-demand band structures and transport properties, or photosensitizers with broadband photon absorption. Owing to the GRMs intrinsic flexibility, we also envision applications such as wearable energy devices and energy harvesting from water or gas flows. Additionally, because GRMs can perform different functions, they may enable the realization of affordable energy systems with integrated conversion, storage, and sensing modules. In the future, it might be possible to target flexible photovoltaic cells with efficiencies of 12% and cost of  $\sim 0.5\text{€}/\text{W}_{\text{peak}}$  (peak power output), fuel cells with 10 kW per gram of platinum, and energy storage devices with an energy density of at least 250 Wh/kg and cyclability up to 5000 cycles for batteries and a power density of 100kW/kg for supercapacitors. For hydrogen storage, the challenge is to achieve a gravimetric storage of 5.5%.

### REFERENCES AND NOTES

1. A. Peigney, Ch. Laurent, E. Flahaut, R. R. Bacsa, A. Rousset, Specific surface area of carbon nanotubes and bundles of carbon nanotubes. *Carbon* 39, 507–514 (2001). doi: 10.1016/S0008-6223(00)00155-X

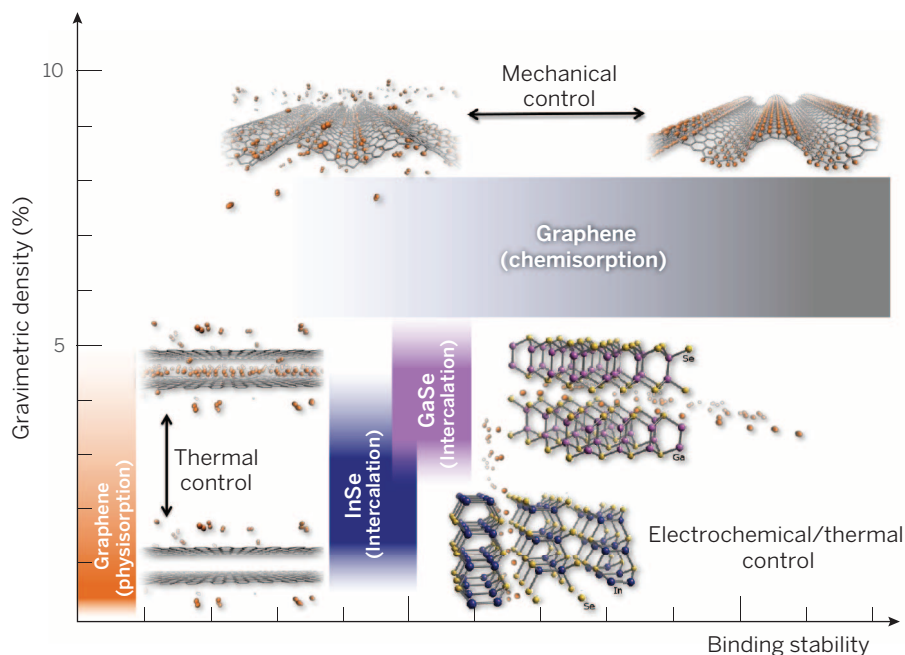


**Fig. 5. Hydrogen storage in GRMs.** The bands indicate the gravimetric density and binding stability (the log of the desorption energy) of different GRMs and for different adsorption mechanisms. In the case of graphene, two different storage procedures are illustrated, based on physisorption or chemisorption, with uptake/release controlled thermally and mechanically, respectively.

2. J. B. Donnet, R. C. Bansal, M.-J. Wang, *Carbon Black Science and Technology* (Marcel Dekker, New York, 1993).
3. Y. Zhu *et al.*, Carbon-based supercapacitors produced by activation of graphene. *Science* **332**, 1537–1541 (2011). doi: [10.1126/science.1200770](https://doi.org/10.1126/science.1200770); pmid: [21566159](https://pubmed.ncbi.nlm.nih.gov/21566159/)
4. A. K. Geim, K. S. Novoselov, The rise of graphene. *Nat. Mater.* **6**, 183–191 (2007). doi: [10.1038/nmat1849](https://doi.org/10.1038/nmat1849); pmid: [17330084](https://pubmed.ncbi.nlm.nih.gov/17330084/)
5. C. Lee, X. Wei, J. W. Kysar, J. Hone, Measurement of the elastic properties and intrinsic strength of monolayer graphene. *Science* **321**, 385–388 (2008). doi: [10.1126/science.1157996](https://doi.org/10.1126/science.1157996); pmid: [18635798](https://pubmed.ncbi.nlm.nih.gov/18635798/)
6. S. Park, R. S. Ruoff, Chemical methods for the production of graphenes. *Nat. Nanotechnol.* **4**, 217–224 (2009). doi: [10.1038/nnano.2009.58](https://doi.org/10.1038/nnano.2009.58); pmid: [19350030](https://pubmed.ncbi.nlm.nih.gov/19350030/)
7. F. Bonaccorso *et al.*, Production and processing of graphene and 2d crystals. *Mater. Today* **15**, 564–589 (2012). doi: [10.1016/j.s31369-7021\(13\)70014-2](https://doi.org/10.1016/j.s31369-7021(13)70014-2)
8. D. C. Elias *et al.*, Control of graphene's properties by reversible hydrogenation: Evidence for graphane. *Science* **323**, 610–613 (2009). doi: [10.1126/science.1167130](https://doi.org/10.1126/science.1167130); pmid: [19179524](https://pubmed.ncbi.nlm.nih.gov/19179524/)
9. V. Tozzini, V. Pellegrini, Reversible hydrogen storage by controlled buckling of graphene layers. *J. Phys. Chem. C* **115**, 25523–25528 (2011). doi: [10.1021/jp208262r](https://doi.org/10.1021/jp208262r)
10. L. Britnell *et al.*, Strong light-matter interactions in heterostructures of atomically thin films. *Science* **340**, 1311–1314 (2013). doi: [10.1126/science.1235547](https://doi.org/10.1126/science.1235547); pmid: [23641062](https://pubmed.ncbi.nlm.nih.gov/23641062/)
11. M. Naguib *et al.*, MXene: A promising transition metal carbide anode for lithium-ion batteries. *Electrochem. Commun.* **16**, 61–64 (2012). doi: [10.1016/j.elecom.2012.01.002](https://doi.org/10.1016/j.elecom.2012.01.002)
12. M. R. Lukatskaya *et al.*, Cation intercalation and high volumetric capacitance of two-dimensional titanium carbide. *Science* **341**, 1502–1505 (2013). doi: [10.1126/science.1241488](https://doi.org/10.1126/science.1241488); pmid: [24072919](https://pubmed.ncbi.nlm.nih.gov/24072919/)
13. Q. Hu *et al.*, MXene: A new family of promising hydrogen storage medium. *J. Phys. Chem. A* **117**, 14253–14260 (2013). doi: [10.1021/jp409585v](https://doi.org/10.1021/jp409585v); pmid: [24261885](https://pubmed.ncbi.nlm.nih.gov/24261885/)
14. Q. Xiang, J. Yu, M. Jaroniec, Synergistic effect of MoS<sub>2</sub> and graphene as cocatalysts for enhanced photocatalytic H<sub>2</sub> production activity of TiO<sub>2</sub> nanoparticles. *J. Am. Chem. Soc.* **134**, 6575–6578 (2012). doi: [10.1021/ja302846n](https://doi.org/10.1021/ja302846n); pmid: [22458309](https://pubmed.ncbi.nlm.nih.gov/22458309/)
15. Q. Cheng *et al.*, Graphene and carbon nanotube composite electrodes for supercapacitors with ultra-high energy density. *Phys. Chem. Chem. Phys.* **13**, 17615–17624 (2011). doi: [10.1039/c1cp21910c](https://doi.org/10.1039/c1cp21910c); pmid: [21887427](https://pubmed.ncbi.nlm.nih.gov/21887427/)
16. A. C. Ferrari *et al.*, Science and technology roadmap for graphene, related two-dimensional crystals, and hybrid systems. *Nanoscale* **10.1039/C4NR01600A** (2014). doi: [10.1039/C4NR01600A](https://doi.org/10.1039/C4NR01600A)
17. Y. Hernandez *et al.*, High-yield production of graphene by liquid-phase exfoliation of graphite. *Nat. Nanotechnol.* **3**, 563–568 (2008). doi: [10.1038/nnano.2008.215](https://doi.org/10.1038/nnano.2008.215); pmid: [18772919](https://pubmed.ncbi.nlm.nih.gov/18772919/)
18. K. R. Paton *et al.*, Scalable production of large quantities of defect-free few-layer graphene by shear exfoliation in liquids. *Nat. Mater.* **13**, 624–630 (2014). doi: [10.1038/nmat3944](https://doi.org/10.1038/nmat3944); pmid: [24747780](https://pubmed.ncbi.nlm.nih.gov/24747780/)
19. J. Cai *et al.*, Atomically precise bottom-up fabrication of graphene nanoribbons. *Nature* **466**, 470–473 (2010). doi: [10.1038/nature09211](https://doi.org/10.1038/nature09211); pmid: [20651687](https://pubmed.ncbi.nlm.nih.gov/20651687/)
20. D. Chapin, C. Fuller, G. Pearson, A new silicon p-n junction photocell for converting solar radiation into electrical power. *J. Appl. Phys.* **25**, 676 (1954). doi: [10.1063/1.1721711](https://doi.org/10.1063/1.1721711)
21. F. Bonaccorso, Z. Sun, T. Hasan, A. C. Ferrari, Graphene photonics and optoelectronics. *Nat. Photonics* **4**, 611–622 (2010). doi: [10.1038/nphoton.2010.186](https://doi.org/10.1038/nphoton.2010.186)
22. M. A. Green, M. J. Keevers, Optical properties of intrinsic silicon at 300 K. *Prog. Photovolt. Res. Appl.* **3**, 189–192 (1995). doi: [10.1002/ppa.4670030303](https://doi.org/10.1002/ppa.4670030303)
23. L. Gomez De Arco *et al.*, Continuous, highly flexible, and transparent graphene films by chemical vapor deposition for organic photovoltaics. *ACS Nano* **4**, 2865–2873 (2010). doi: [10.1021/nn901587x](https://doi.org/10.1021/nn901587x); pmid: [20394355](https://pubmed.ncbi.nlm.nih.gov/20394355/)
24. Y. Wu *et al.*, Graphene transparent conductive electrodes for highly efficient silicon nanostructures-based hybrid heterojunction solar cells. *J. Phys. Chem. C* **117**, 11968–11976 (2013). doi: [10.1021/jp402529c](https://doi.org/10.1021/jp402529c)
25. W. Hong, Y. Xu, G. Lu, C. Li, G. Shi, Transparent graphene/PEDOT-PSS composite films as counter electrodes of dye-sensitized solar cells. *Electrochem. Commun.* **10**, 1555–1558 (2008). doi: [10.1016/j.elecom.2008.08.007](https://doi.org/10.1016/j.elecom.2008.08.007)
26. L. Kavan, J.-H. Yum, M. Grätzel, Graphene nanoplatelets outperforming platinum as the electrocatalyst in co-bipyridine-mediated dye-sensitized solar cells. *Nano Lett.* **11**, 5501–5506 (2011). doi: [10.1021/nl203329c](https://doi.org/10.1021/nl203329c); pmid: [22103554](https://pubmed.ncbi.nlm.nih.gov/22103554/)
27. S. Mathew *et al.*, Dye-sensitized solar cells with 13% efficiency achieved through the molecular engineering of porphyrin sensitizers. *Nat. Chem.* **6**, 242–247 (2014). doi: [10.1038/nchem.1861](https://doi.org/10.1038/nchem.1861); pmid: [24557140](https://pubmed.ncbi.nlm.nih.gov/24557140/)
28. X. Yan, X. Cui, B. Li, L. S. Li, Large, solution-processable graphene quantum dots as light absorbers for photovoltaics. *Nano Lett.* **10**, 1869–1873 (2010). doi: [10.1021/nl101060h](https://doi.org/10.1021/nl101060h); pmid: [20377198](https://pubmed.ncbi.nlm.nih.gov/20377198/)
29. B. Poudel *et al.*, High-thermoelectric performance of nanostructured bismuth antimony telluride bulk alloys. *Science* **320**, 634–638 (2008). doi: [10.1126/science.1156446](https://doi.org/10.1126/science.1156446); pmid: [18356488](https://pubmed.ncbi.nlm.nih.gov/18356488/)
30. I.-Y. Jeon *et al.*, Facile, scalable synthesis of edge-halogenated graphene nanoplatelets as efficient metal-free electrocatalysts for oxygen reduction reaction. *Sci. Rep.* **3**, 1810 (2013). doi: [10.1038/srep01810](https://doi.org/10.1038/srep01810); pmid: [23736800](https://pubmed.ncbi.nlm.nih.gov/23736800/)
31. H. A. Liebhafsky, E. J. Cairns, *Fuel Cells and Fuel Batteries: A Guide to Their Research and Development* (Wiley, New York, 1969).
32. M. A. Green, K. Emery, Y. Hishikawa, W. Warta, E. D. Dunlop, Solar cell efficiency tables (version 42). *Prog. Photovolt. Res. Appl.* **21**, 827 (2013). doi: [10.1002/ppa.2352](https://doi.org/10.1002/ppa.2352)
33. H. Hoppe, N. S. Sariciffici, Organic solar cells: An overview. *J. Mater. Res.* **19**, 1925 (2004). doi: [10.1557/JMR.2004.0252](https://doi.org/10.1557/JMR.2004.0252)
34. B. O'Regan, M. Grätzel, A low-cost, high-efficiency solar cell based on dye-sensitized colloidal TiO<sub>2</sub> films. *Nature* **353**, 737–740 (1991). doi: [10.1038/353737a0](https://doi.org/10.1038/353737a0)
35. J. G. Radich, R. Dwyer, P. V. Kamat, CuS reduced graphene oxide composite for high-efficiency quantum dot solar cells. Overcoming the redox limitations of S<sub>2</sub><sup>2-</sup>/S<sub>2</sub><sup>2-</sup> at the counter electrode. *J. Phys. Chem. Lett.* **2**, 2453–2460 (2011). doi: [10.1021/jz201064k](https://doi.org/10.1021/jz201064k)
36. [www.heliatek.com/newscenter/latest\\_news/neuer-weltrekord-fur-organische-solarzellen-heliatek-behauptet-sich-mit-12-zelleffizienz-als-technologiefuhrer/?lang=en](http://www.heliatek.com/newscenter/latest_news/neuer-weltrekord-fur-organische-solarzellen-heliatek-behauptet-sich-mit-12-zelleffizienz-als-technologiefuhrer/?lang=en)
37. A. Kojima, K. Teshima, Y. Shirai, T. Miyasaka, Organometal halide perovskites as visible-light sensitizers for photovoltaic cells. *J. Am. Chem. Soc.* **131**, 6050–6051 (2009). doi: [10.1021/ja809598r](https://doi.org/10.1021/ja809598r); pmid: [19366264](https://pubmed.ncbi.nlm.nih.gov/19366264/)
38. M. Liu, M. B. Johnston, H. J. Snaith, Efficient planar heterojunction perovskite solar cells by vapour deposition. *Nature* **501**, 395–398 (2013). doi: [10.1038/nature12509](https://doi.org/10.1038/nature12509); pmid: [24025775](https://pubmed.ncbi.nlm.nih.gov/24025775/)
39. [www.nrel.gov/ncpv/images/efficiency\\_chart.jpg](http://www.nrel.gov/ncpv/images/efficiency_chart.jpg)
40. X. Wang, L. Zhi, K. Müllen, Transparent, conductive graphene electrodes for dye-sensitized solar cells. *Nano Lett.* **8**, 323–327 (2008). doi: [10.1021/nl072838r](https://doi.org/10.1021/nl072838r); pmid: [18069877](https://pubmed.ncbi.nlm.nih.gov/18069877/)
41. N. Yang, J. Zhai, D. Wang, Y. Chen, L. Jiang, Two-dimensional graphene bridges enhanced photoinduced charge transport in dye-sensitized solar cells. *ACS Nano* **4**, 887–894 (2010). doi: [10.1021/nr901660v](https://doi.org/10.1021/nr901660v); pmid: [20088539](https://pubmed.ncbi.nlm.nih.gov/20088539/)
42. F. Xu *et al.*, Graphene scaffolds enhanced photogenerated electron transport in ZnO photoanodes for high-efficiency dye-sensitized solar cells. *J. Phys. Chem. C* **117**, 8619–8627 (2013). doi: [10.1021/jp312379b](https://doi.org/10.1021/jp312379b)
43. J. D. Roy-Mayhew, D. J. Bozym, C. Punckt, I. A. Aksay, Functionalized graphene as a catalytic counter electrode in dye-sensitized solar cells. *ACS Nano* **4**, 6203–6211 (2010). doi: [10.1021/nl1016428](https://doi.org/10.1021/nl1016428); pmid: [20939517](https://pubmed.ncbi.nlm.nih.gov/20939517/)
44. M. W. Rowell, M. D. McGehee, Transparent electrode requirements for thin film solar cell modules. *Energy Environ. Sci.* **4**, 131 (2011). doi: [10.1039/c0ee00373e](https://doi.org/10.1039/c0ee00373e)
45. J. Kalowekamo, E. Baker, Estimating the manufacturing cost of purely organic solar cells. *Sol. Energy* **83**, 1224–1231 (2009). doi: [10.1016/j.solener.2009.02.003](https://doi.org/10.1016/j.solener.2009.02.003)
46. X. Li *et al.*, Graphene-on-silicon Schottky junction solar cells. *Adv. Mater.* **22**, 2743–2748 (2010). doi: [10.1002/adma.200904383](https://doi.org/10.1002/adma.200904383); pmid: [20379996](https://pubmed.ncbi.nlm.nih.gov/20379996/)
47. Y. Hao *et al.*, The role of surface oxygen in the growth of large single-crystal graphene on copper. *Science* **342**, 720–723 (2013). doi: [10.1126/science.1243879](https://doi.org/10.1126/science.1243879); pmid: [24158906](https://pubmed.ncbi.nlm.nih.gov/24158906/)
48. T. Kobayashi *et al.*, Production of a 100-m-long high-quality graphene transparent conductive film by roll-to-roll chemical vapor deposition and transfer process. *Appl. Phys. Lett.* **102**, 023112 (2013). doi: [10.1063/1.4776707](https://doi.org/10.1063/1.4776707)
49. S. Bae *et al.*, Roll-to-roll production of 30-inch graphene films for transparent electrodes. *Nat. Nanotechnol.* **5**, 574–578 (2010). doi: [10.1038/nano.2010.132](https://doi.org/10.1038/nano.2010.132); pmid: [20562870](https://pubmed.ncbi.nlm.nih.gov/20562870/)
50. X. Miao *et al.*, High efficiency graphene solar cells by chemical doping. *Nano Lett.* **12**, 2745–2750 (2012). doi: [10.1021/nl204414u](https://doi.org/10.1021/nl204414u); pmid: [22554195](https://pubmed.ncbi.nlm.nih.gov/22554195/)
51. Y. Zhu, Z. Sun, Z. Yan, Z. Jin, J. M. Tour, Rational design of hybrid graphene films for high-performance transparent electrodes. *ACS Nano* **5**, 6472–6479 (2011). doi: [10.1021/nm201696g](https://doi.org/10.1021/nm201696g); pmid: [21774533](https://pubmed.ncbi.nlm.nih.gov/21774533/)
52. H. Peng *et al.*, Topological insulator nanostructures for near-infrared transparent flexible electrodes. *Nat. Chem.* **4**, 281–286 (2012). doi: [10.1038/nchem.1277](https://doi.org/10.1038/nchem.1277); pmid: [22437712](https://pubmed.ncbi.nlm.nih.gov/22437712/)
53. M. K. Nazeeuddin *et al.*, Conversion of light to electricity by cis-XZbis(2,2'-bipyridyl)-4,4'-dicarboxylate]ruthenium(II) charge-transfer sensitizers (X = Cl<sup>-</sup>, Br<sup>-</sup>, I<sup>-</sup>, CN<sup>-</sup>, and SCN<sup>-</sup>) on nanocrystalline titanium dioxide electrodes. *J. Am. Chem. Soc.* **115**, 6382–6390 (1993). doi: [10.1021/ja00067a063](https://doi.org/10.1021/ja00067a063)
54. J. H. Yum *et al.*, Efficient far red sensitization of nanocrystalline TiO<sub>2</sub> films by an unsymmetrical squaraine dye. *J. Am. Chem. Soc.* **129**, 10320–10321 (2007). doi: [10.1021/ja0731470](https://doi.org/10.1021/ja0731470); pmid: [17672464](https://pubmed.ncbi.nlm.nih.gov/17672464/)
55. H. X. Wang, Q. Wang, K. G. Zhou, H. L. Zhang, Graphene in light: Design, synthesis and applications of photo-active graphene and graphene-like materials. *Small* **9**, 1266–1283 (2013). doi: [10.1002/sml.201203040](https://doi.org/10.1002/sml.201203040); pmid: [23554268](https://pubmed.ncbi.nlm.nih.gov/23554268/)
56. V. Yong, J. M. Tour, Theoretical efficiency of nanostructured graphene-based photovoltaics. *Small* **6**, 313–318 (2010). doi: [10.1002/sml.200901364](https://doi.org/10.1002/sml.200901364); pmid: [19943249](https://pubmed.ncbi.nlm.nih.gov/19943249/)
57. M. Bernardi, M. Palummo, J. C. Grossman, Extraordinary sunlight absorption and one nanometer thick photovoltaics using two-dimensional monolayer materials. *Nano Lett.* **13**, 3664–3670 (2013). doi: [10.1021/nl401544y](https://doi.org/10.1021/nl401544y); pmid: [23759010](https://pubmed.ncbi.nlm.nih.gov/23759010/)
58. T. J. Echtermeyer *et al.*, Strong plasmonic enhancement of photovoltage in graphene. *Nat. Commun.* **2**, 458 (2011). doi: [10.1038/ncomms1464](https://doi.org/10.1038/ncomms1464); pmid: [21878912](https://pubmed.ncbi.nlm.nih.gov/21878912/)
59. M. D. Stoller, S. Park, Y. Zhu, J. An, R. S. Ruoff, Graphene-based ultracapacitors. *Nano Lett.* **8**, 3498–3502 (2008). doi: [10.1021/nl802558y](https://doi.org/10.1021/nl802558y); pmid: [18788793](https://pubmed.ncbi.nlm.nih.gov/18788793/)
60. J. T.-W. Wang *et al.*, Low-temperature processed electron collection layers of graphene/TiO<sub>2</sub> nanocomposites in thin film perovskite solar cells. *Nano Lett.* **14**, 724–730 (2014). doi: [10.1021/nl403997a](https://doi.org/10.1021/nl403997a); pmid: [24341922](https://pubmed.ncbi.nlm.nih.gov/24341922/)
61. S.-S. Li, K.-H. Tu, C.-C. Lin, C.-W. Chen, M. Chhowalla, Solution-processable graphene oxide as an efficient hole transport layer in polymer solar cells. *ACS Nano* **4**, 3169–3174 (2010). doi: [10.1021/nl100551j](https://doi.org/10.1021/nl100551j); pmid: [20481512](https://pubmed.ncbi.nlm.nih.gov/20481512/)
62. Y.-J. Jeon, J.-M. Yun, D.-Y. Kim, S.-I. Na, S.-S. Kim, High-performance polymer solar cells with moderately reduced graphene oxide as an efficient hole transporting layer. *Sol. Energy Mater. Sol. Cells* **95**, 96–102 (2012). doi: [10.1016/j.solmat.2012.05.024](https://doi.org/10.1016/j.solmat.2012.05.024)
63. M. Li *et al.*, Graphene quantum dots as the hole transport layer material for high-performance organic solar cells. *Phys. Chem. Chem. Phys.* **15**, 18973–18978 (2013). doi: [10.1039/c3cp53283f](https://doi.org/10.1039/c3cp53283f); pmid: [24097209](https://pubmed.ncbi.nlm.nih.gov/24097209/)
64. H. Choi, H. Kim, S. Hwang, W. Choi, M. Jeon, Dye-sensitized solar cells using graphene-based carbon nano composite as counter electrode. *Sol. Energy Mater. Sol. Cells* **95**, 323–325 (2010). doi: [10.1016/j.solmat.2010.04.044](https://doi.org/10.1016/j.solmat.2010.04.044)
65. M. Wu *et al.*, Economical and effective sulfide catalysts for dye-sensitized solar cells as counter electrodes. *Phys. Chem. Chem. Phys.* **13**, 19298–19301 (2011). doi: [10.1039/c1cp22819f](https://doi.org/10.1039/c1cp22819f); pmid: [21984309](https://pubmed.ncbi.nlm.nih.gov/21984309/)
66. J.-Y. Lin, C.-Y. Chan, S.-W. Chou, Electrophoretic deposition of transparent MoS<sub>2</sub>-graphene nanosheet composite films as counter electrodes in dye-sensitized solar cells. *Chem. Commun. (Camb.)* **49**, 1440–1442 (2013). doi: [10.1039/c2cc38658e](https://doi.org/10.1039/c2cc38658e); pmid: [23321629](https://pubmed.ncbi.nlm.nih.gov/23321629/)
67. J. Liang, H. Bi, D. Wan, F. Huang, Novel Cu nanowires/graphene as the back contact for CdTe solar cells. *Adv. Funct. Mater.* **22**, 1267–1271 (2012). doi: [10.1002/adfm.201102809](https://doi.org/10.1002/adfm.201102809)
68. E. Shi *et al.*, Colloidal antireflection coating improves graphene-silicon solar cells. *Nano Lett.* **13**, 1776–1781 (2013). pmid: [23517083](https://pubmed.ncbi.nlm.nih.gov/23517083/)
69. F. J. DiSalvo, Thermoelectric cooling and power generation. *Science* **285**, 703–706 (1999). doi: [10.1126/science.285.5428.703](https://doi.org/10.1126/science.285.5428.703); pmid: [10426986](https://pubmed.ncbi.nlm.nih.gov/10426986/)
70. G. A. Slack, *CRC Handbook of Thermoelectrics*, D. M. Rowe, Ed. (CRC Press, Boca Raton, FL, 1995).
71. R. Venkatasubramanian, E. Siivola, T. Colpitts, B. O'Quinn, Thin-film thermoelectric devices with high room-temperature figures of merit. *Nature* **413**, 597–602 (2001). doi: [10.1038/35098012](https://doi.org/10.1038/35098012); pmid: [11595940](https://pubmed.ncbi.nlm.nih.gov/11595940/)
72. C. B. Vining, An inconvenient truth about thermoelectrics. *Nat. Mater.* **8**, 83–85 (2009). doi: [10.1038/nmat2361](https://doi.org/10.1038/nmat2361); pmid: [19165205](https://pubmed.ncbi.nlm.nih.gov/19165205/)

73. A. A. Balandin *et al.*, Superior thermal conductivity of single-layer graphene. *Nano Lett.* **8**, 902–907 (2008). doi: [10.1021/nl0731872](https://doi.org/10.1021/nl0731872); pmid: [18284217](https://pubmed.ncbi.nlm.nih.gov/18284217/)
74. J. Haskins *et al.*, Control of thermal and electronic transport in defect-engineered graphene nanoribbons. *ACS Nano* **5**, 3779–3787 (2011). doi: [10.1021/nm200114p](https://doi.org/10.1021/nm200114p); pmid: [21452884](https://pubmed.ncbi.nlm.nih.gov/21452884/)
75. S. Chen *et al.*, Thermal conductivity of isotopically modified graphene. *Nat. Mater.* **11**, 203–207 (2012). doi: [10.1038/nmat3207](https://doi.org/10.1038/nmat3207); pmid: [22231598](https://pubmed.ncbi.nlm.nih.gov/22231598/)
76. T. Gunst, T. Markussen, A.-P. Jauho, M. Brandbyge, Thermoelectric properties of finite graphene antidot lattices. *Phys. Rev. B* **84**, 155449 (2011). doi: [10.1103/PhysRevB.84.155449](https://doi.org/10.1103/PhysRevB.84.155449)
77. H. Sevinçli, C. Sevik, T. Cain, G. Cuniberti, A bottom-up route to enhance thermoelectric figures of merit in graphene nanoribbons. *Sci. Rep.* **3**, 1228 (2013). pmid: [23390578](https://pubmed.ncbi.nlm.nih.gov/23390578/)
78. S. Hu *et al.*, Proton transport through one-atom-thick crystals. *Nature* **516**, 227–230 (2014). doi: [10.1038/nature14015](https://doi.org/10.1038/nature14015)
79. L. Dong, R. R. S. Gari, Z. Li, M. M. Craig, S. Hou, Graphene-supported platinum and platinum–ruthenium nanoparticles with high electrocatalytic activity for methanol and ethanol oxidation. *Carbon* **48**, 781–787 (2010). doi: [10.1016/j.carbon.2009.10.027](https://doi.org/10.1016/j.carbon.2009.10.027)
80. E. Yoo *et al.*, Enhanced electrocatalytic activity of Pt subnanoclusters on graphene nanosheet surface. *Nano Lett.* **9**, 2255–2259 (2009). doi: [10.1021/nl900397t](https://doi.org/10.1021/nl900397t); pmid: [19405511](https://pubmed.ncbi.nlm.nih.gov/19405511/)
81. A. Tarancon, M. Burriel, J. Santiso, S. J. Skinner, J. A. Kilner, Advances in layered oxide cathodes for intermediate temperature solid oxide fuel cells. *J. Mater. Chem.* **20**, 3799 (2010). doi: [10.1039/b922430k](https://doi.org/10.1039/b922430k)
82. D. Linden, T.B. Reddy, *Handbook of Batteries* (McGraw Hill, New York, ed. 4, 2010)
83. G. Wang, X. Shen, J. Yao, J. Park, Graphene nanosheets for enhanced lithium storage in lithium ion batteries. *Carbon* **47**, 2049–2053 (2009). doi: [10.1016/j.carbon.2009.03.053](https://doi.org/10.1016/j.carbon.2009.03.053)
84. G. Zhou, F. Li, H.-M. Cheng, Progress in flexible lithium batteries and future prospects. *Energy Environ. Sci.* **7**, 1307 (2014). doi: [10.1039/c3ee43182g](https://doi.org/10.1039/c3ee43182g)
85. A. Burke, M. Miller, H. Zhao, “Ultracapacitors in Hybrid Vehicle Applications: Testing of New High Power Devices and Prospects for Increased Energy Density.” Institute of Transportation Studies, University of California, Davis, Research Report UCD-ITS-RR-12-06 (2012).
86. P. G. Bruce, S. A. Freunberger, L. J. Hardwick, J.-M. Tarascon, Li-O<sub>2</sub> and Li-S batteries with high energy storage. *Nat. Mater.* **11**, 19–29 (2012). doi: [10.1038/nmat3191](https://doi.org/10.1038/nmat3191); pmid: [22169914](https://pubmed.ncbi.nlm.nih.gov/22169914/)
87. K. C. Divya, J. Ostergaard, Battery energy storage technology for power systems—An overview. *Electr. Power Syst. Res.* **79**, 511–520 (2009). doi: [10.1016/j.epsr.2008.09.017](https://doi.org/10.1016/j.epsr.2008.09.017)
88. A. K. Padhi, K. S. Nanjundaswamy, J. B. Goodenough, Phospho-olivines as positive-electrode materials for rechargeable lithium batteries. *J. Electrochem. Soc.* **144**, 1188 (1997). doi: [10.1149/1.1837571](https://doi.org/10.1149/1.1837571)
89. T. Ozkuku, Y. Makimura, Layered lithium insertion material of LiC<sub>12</sub>Ni<sub>1/3</sub>Mn<sub>1/3</sub>O<sub>2</sub> for lithium-ion batteries. *Chem. Lett.* **30**, 642–643 (2001). doi: [10.1246/cl.2001.642](https://doi.org/10.1246/cl.2001.642)
90. M. M. Thackeray, W. David, P. G. Bruce, J. B. Goodenough, Lithium insertion into manganese spinels. *Mater. Res. Bull.* **18**, 461–472 (1983). doi: [10.1016/0025-5408\(83\)90138-1](https://doi.org/10.1016/0025-5408(83)90138-1)
91. J. Hassoun *et al.*, An advanced lithium-ion battery based on a graphene anode and a lithium iron phosphate cathode. *Nano Lett.* **14**, 4901–4906 (2014). doi: [10.1021/nl502429m](https://doi.org/10.1021/nl502429m); pmid: [25026051](https://pubmed.ncbi.nlm.nih.gov/25026051/)
92. B. Lung-Hao Hu, F. Y. Wu, C. T. Lin, A. N. Khlobystov, L. J. Li, Graphene-modified LiFePO<sub>4</sub> cathode for lithium ion battery beyond theoretical capacity. *Nat. Commun.* **4**, 1687 (2013). doi: [10.1038/ncomms2705](https://doi.org/10.1038/ncomms2705); pmid: [23575691](https://pubmed.ncbi.nlm.nih.gov/23575691/)
93. E. Yoo *et al.*, Large reversibly Li storage of graphene nanosheet families for use in rechargeable lithium ion batteries. *Nano Lett.* **8**, 2277–2282 (2008). doi: [10.1021/nl800957b](https://doi.org/10.1021/nl800957b); pmid: [18651781](https://pubmed.ncbi.nlm.nih.gov/18651781/)
94. H. Wang *et al.*, LiMn<sub>2</sub>FePO<sub>4</sub> nanorods grown on graphene sheets for ultrahigh-rate-performance lithium ion batteries. *Angew. Chem. Int. Ed.* **123**, 7502–7506 (2011). doi: [10.1002/ange.201103163](https://doi.org/10.1002/ange.201103163)
95. H. Kim *et al.*, Graphene-based hybrid electrode material for high-power lithium-ion batteries. *J. Electrochem. Soc.* **158**, A930 (2011). doi: [10.1149/1.3599632](https://doi.org/10.1149/1.3599632)
96. S.-M. Bak *et al.*, Spinel LiMn<sub>2</sub>O<sub>4</sub>/reduced graphene oxide hybrid for high rate lithium ion batteries. *J. Mater. Chem.* **21**, 17309 (2011). doi: [10.1039/c1jm13741g](https://doi.org/10.1039/c1jm13741g)
97. S. Yang, X. Feng, S. Ivanovici, K. Müllen, Fabrication of graphene-encapsulated oxide nanoparticles: Towards high-performance anode materials for lithium storage. *Angew. Chem. Int. Ed. Engl.* **49**, 8408–8411 (2010). doi: [10.1002/anie.201003485](https://doi.org/10.1002/anie.201003485); pmid: [20836109](https://pubmed.ncbi.nlm.nih.gov/20836109/)
98. G. Zhou *et al.*, Graphene-wrapped Fe<sub>3</sub>O<sub>4</sub> anode material with improved reversible capacity and cyclic stability for lithium ion batteries. *Chem. Mater.* **22**, 5306–5313 (2010). doi: [10.1021/cm101532x](https://doi.org/10.1021/cm101532x)
99. Y. Shi *et al.*, Hollow structured Li<sub>2</sub>VO<sub>4</sub> wrapped with graphene nanosheets in situ prepared by a one-pot template-free method as an anode for lithium-ion batteries. *Nano Lett.* **13**, 4715–4720 (2013). doi: [10.1021/nl402237u](https://doi.org/10.1021/nl402237u); pmid: [24024651](https://pubmed.ncbi.nlm.nih.gov/24024651/)
100. X. Zhao, C. M. Hayner, M. C. Kung, H. H. Kung, In-plane vacancy-enabled high-power Si–graphene composite electrode for lithium-ion batteries. *Adv. Energy Mater.* **1**, 1079–1084 (2011). doi: [10.1002/aenm.201100426](https://doi.org/10.1002/aenm.201100426)
101. B. Amundsen, J. Paulsen, Novel lithium-ion cathode materials based on layered manganese oxides. *Adv. Mater.* **13**, 943–956 (2001). doi: [10.1002/1521-4095\(200107\)13:12/13<943::AID-ADMA943>3.0.CO;2-J](https://doi.org/10.1002/1521-4095(200107)13:12/13<943::AID-ADMA943>3.0.CO;2-J)
102. M. S. Whittingham, Electrical energy storage and intercalation chemistry. *Science* **192**, 1126–1127 (1976). doi: [10.1126/science.192.4244.1126](https://doi.org/10.1126/science.192.4244.1126); pmid: [17748676](https://pubmed.ncbi.nlm.nih.gov/17748676/)
103. G. Du *et al.*, Superior stability and high capacity of restacked molybdenum disulfide as anode material for lithium ion batteries. *Chem. Commun. (Camb.)* **46**, 1106–1108 (2010). doi: [10.1039/b920277c](https://doi.org/10.1039/b920277c); pmid: [20126728](https://pubmed.ncbi.nlm.nih.gov/20126728/)
104. J. T. Jang *et al.*, Ultrathin zirconium disulfide nanodiscs. *J. Am. Chem. Soc.* **133**, 7636–7639 (2011). doi: [10.1021/ja200400n](https://doi.org/10.1021/ja200400n); pmid: [21539379](https://pubmed.ncbi.nlm.nih.gov/21539379/)
105. K. Shiva, H. S. S. R. Matte, H. B. Reajendra, A. J. Bhattacharyya, C. N. R. Rao, Employing synergistic interactions between few-layer WS<sub>2</sub> and reduced graphene oxide to improve lithium storage, cyclability and rate capability of Li-ion batteries. *Nano Energy* **2**, 787–793 (2013). doi: [10.1016/j.nanoen.2013.02.001](https://doi.org/10.1016/j.nanoen.2013.02.001)
106. B. E. Conway, *Electrochemical Supercapacitors: Scientific Fundamentals and Technological Applications* (Plenum Publishers, New York, 1999).
107. M. Stoller *et al.*, Interfacial capacitance of single layer graphene. *Energy Environ. Sci.* **4**, 4685 (2011). doi: [10.1039/c1ee02322e](https://doi.org/10.1039/c1ee02322e)
108. J. W. Longa *et al.*, Asymmetric electrochemical capacitors—Stretching the limits of aqueous electrolytes. *MRS Bull.* **36**, 513–522 (2011). doi: [10.1557/mrs.2011.137](https://doi.org/10.1557/mrs.2011.137)
109. M. D. Stoller, R. S. Ruoff, Best practice methods for determining an electrode material’s performance for ultracapacitors. *Energy Environ. Sci.* **3**, 1294 (2010). doi: [10.1039/c0ee00074d](https://doi.org/10.1039/c0ee00074d)
110. Y. Gogotsi, P. Simon, Materials science. True performance metrics in electrochemical energy storage. *Science* **334**, 917–918 (2011). doi: [10.1126/science.1213003](https://doi.org/10.1126/science.1213003); pmid: [22096182](https://pubmed.ncbi.nlm.nih.gov/22096182/)
111. Y. W. Zhu *et al.*, Microwave assisted exfoliation and reduction of graphite oxide for ultracapacitors. *Carbon* **48**, 2118–2122 (2010). doi: [10.1016/j.carbon.2010.02.001](https://doi.org/10.1016/j.carbon.2010.02.001)
112. S. R. Vivekchand, S. R. Chandra, K. S. Subrahmanyam, A. Govindaraj, C. N. R. Rao, Graphene-based electrochemical supercapacitors. *J. Chem. Soc.* **120**, 9–13 (2008). doi: [10.1007/s12039-008-0002-7](https://doi.org/10.1007/s12039-008-0002-7)
113. Z. Lei, N. Christova, X. S. Zhao, Intercalation of mesoporous carbon spheres between reduced graphene oxide sheets for preparing high-rate supercapacitor electrodes. *Energy Environ. Sci.* **4**, 1866 (2011). doi: [10.1039/c1ee01094h](https://doi.org/10.1039/c1ee01094h)
114. M. A. Pope, S. Korkut, C. Punctat, I. A. Aksay, Supercapacitor electrodes produced through evaporative consolidation of graphene oxide-water-ionic liquid gels. *J. Electrochem. Soc.* **160**, A1653–A1660 (2013). doi: [10.1149/2.0171310jes](https://doi.org/10.1149/2.0171310jes)
115. Y. Li, Z. Li, P. K. Shen, Simultaneous formation of ultrahigh surface area and three-dimensional hierarchical porous graphene-like networks for fast and highly stable supercapacitors. *Adv. Mater.* **25**, 2474–2480 (2013). doi: [10.1002/adma.201205332](https://doi.org/10.1002/adma.201205332); pmid: [24395046](https://pubmed.ncbi.nlm.nih.gov/24395046/)
116. L. Zhang *et al.*, Porous 3D graphene-based bulk materials with exceptional high surface area and excellent conductivity for supercapacitors. *Sci. Rep.* **3**, 1408 (2013). pmid: [23474952](https://pubmed.ncbi.nlm.nih.gov/23474952/)
117. Y. Tao *et al.*, Towards ultrahigh volumetric capacitance: Graphene derived highly dense but porous carbons for supercapacitors. *Sci. Rep.* **3**, 2975 (2013). doi: [10.1038/srep02975](https://doi.org/10.1038/srep02975); pmid: [24131954](https://pubmed.ncbi.nlm.nih.gov/24131954/)
118. X. Yang, C. Cheng, Y. Wang, L. Qiu, D. Li, Liquid-mediated dense integration of graphene materials for compact capacitive energy storage. *Science* **341**, 534–537 (2013). doi: [10.1126/science.1239089](https://doi.org/10.1126/science.1239089); pmid: [23908233](https://pubmed.ncbi.nlm.nih.gov/23908233/)
119. W.-Y. Tsai *et al.*, Outstanding performance of activated graphene based supercapacitors in ionic liquid electrolyte from –50 to 80 °C. *Nano Energy* **2**, 403–411 (2013). doi: [10.1016/j.nanoen.2012.11.006](https://doi.org/10.1016/j.nanoen.2012.11.006)
120. R. S. Borges *et al.*, Supercapacitor operating at 200 degrees celsius. *Sci. Rep.* **3**, 2572 (2013). doi: [10.1038/srep02572](https://doi.org/10.1038/srep02572); pmid: [23999206](https://pubmed.ncbi.nlm.nih.gov/23999206/)
121. F. Beguin, V. Khomenko, E. Raymundo-Pinero, High-energy density graphite/AC capacitor in organic electrolyte. *J. Power Sources* **177**, 643–651 (2008). doi: [10.1016/j.jpowsour.2007.11.101](https://doi.org/10.1016/j.jpowsour.2007.11.101)
122. M. D. Stoller *et al.*, Activated graphene as a cathode material for Li-ion hybrid supercapacitors. *Phys. Chem. Chem. Phys.* **14**, 3388–3391 (2012). doi: [10.1039/c2cp00017b](https://doi.org/10.1039/c2cp00017b); pmid: [22298158](https://pubmed.ncbi.nlm.nih.gov/22298158/)
123. F. Zhang *et al.*, A high-performance supercapacitor-battery hybrid energy storage device based on graphene-enhanced electrode materials with ultrahigh energy density. *Energy Environ. Sci.* **6**, 1623 (2013). doi: [10.1039/c3ee40509e](https://doi.org/10.1039/c3ee40509e)
124. Z. S. Wu *et al.*, High-energy MnO<sub>2</sub> nanowire/graphene and graphene asymmetric electrochemical capacitors. *ACS Nano* **4**, 5835–5842 (2010). doi: [10.1021/nm101754k](https://doi.org/10.1021/nm101754k); pmid: [20857919](https://pubmed.ncbi.nlm.nih.gov/20857919/)
125. Q. Wu, Y. Xu, Z. Yao, A. Liu, G. Shi, Supercapacitors based on flexible graphene/polyaniline nanofiber composite films. *ACS Nano* **4**, 1963–1970 (2010). doi: [10.1021/nm1000035](https://doi.org/10.1021/nm1000035); pmid: [20355733](https://pubmed.ncbi.nlm.nih.gov/20355733/)
126. J. Yang, H. S. Shin, Recent advances in layered transition metal dichalcogenides for hydrogen evolution reaction. *J. Mater. Chem. A* **2**, 5979 (2014). doi: [10.1039/c3ta14151a](https://doi.org/10.1039/c3ta14151a)
127. X. Zheng *et al.*, Space-confined growth of MoS<sub>2</sub> nanosheets within graphite: The layered hybrid of MoS<sub>2</sub> and graphene as an active catalyst for hydrogen evolution reaction. *Chem. Mater.* **26**, 2344–2353 (2014). doi: [10.1021/cm500347r](https://doi.org/10.1021/cm500347r)
128. D. Voiry *et al.*, Conducting MoS<sub>2</sub> nanosheets as catalysts for hydrogen evolution reaction. *Nano Lett.* **13**, 6222–6227 (2013). doi: [10.1021/nl403661s](https://doi.org/10.1021/nl403661s); pmid: [24251828](https://pubmed.ncbi.nlm.nih.gov/24251828/)
129. S. Patchkovskii *et al.*, Graphene nanostructures as tunable storage media for molecular hydrogen. *Proc. Natl. Acad. Sci. U.S.A.* **102**, 10439–10444 (2005). doi: [10.1073/pnas.0501030102](https://doi.org/10.1073/pnas.0501030102); pmid: [16020537](https://pubmed.ncbi.nlm.nih.gov/16020537/)
130. G. K. Dimitrakakis, E. Tylanakis, G. E. Froudakis, Pillared graphene: A new 3-D network structure for enhanced hydrogen storage. *Nano Lett.* **8**, 3166–3170 (2008). doi: [10.1021/nl801417w](https://doi.org/10.1021/nl801417w); pmid: [18800853](https://pubmed.ncbi.nlm.nih.gov/18800853/)
131. G. Srinivas *et al.*, Synthesis of graphene-like nanosheets and their hydrogen adsorption capacity. *Carbon* **48**, 630–635 (2010). doi: [10.1016/j.carbon.2009.10.003](https://doi.org/10.1016/j.carbon.2009.10.003)
132. Y. I. Zhirkov, Z. D. Kovalyuk, M. M. Pyrlja, V. B. Boledzyuk, in *Hydrogen Materials Science and Chemistry of Carbon Nanomaterials series: NATO Security through Science Series A: Chemistry and Biology* (Springer, Netherlands, 2007).
133. G. Kim, S.-H. Jhi, N. Park, M. L. Cohen, S. G. Louie, Optimization of metal dispersion in doped graphitic materials for hydrogen storage. *Phys. Rev. B* **78**, 085408 (2008). doi: [10.1103/PhysRevB.78.085408](https://doi.org/10.1103/PhysRevB.78.085408)
134. S. Goler *et al.*, The influence of graphene curvature on hydrogen adsorption: A study for future hydrogen storage devices. *J. Phys. Chem. C* **117**, 11506–11513 (2013). doi: [10.1021/jp4017536](https://doi.org/10.1021/jp4017536)
135. V. B. Parambath, R. Nagar, K. Sethupathi, S. Ramaprabhu, Investigation of spillover mechanism in palladium decorated hydrogen exfoliated functionalized graphene. *J. Phys. Chem. C* **115**, 15679–15685 (2011). doi: [10.1021/jp202797q](https://doi.org/10.1021/jp202797q)
136. Z. M. Ao, F. M. Peeters, Electric field activated hydrogen dissociative adsorption to nitrogen-doped graphene. *J. Phys. Chem. C* **114**, 14503–14509 (2010). doi: [10.1021/jp103835k](https://doi.org/10.1021/jp103835k)
137. D. W. Boukhvalov, M. I. Katsnelson, Enhancement of chemical activity in corrugated graphene. *J. Phys. Chem. C* **113**, 14176–14178 (2009). doi: [10.1021/jp905702e](https://doi.org/10.1021/jp905702e)
138. M. T. Ong, E. J. Reed, Engineered piezoelectricity in graphene. *ACS Nano* **6**, 1387–1394 (2012). doi: [10.1021/nm204198g](https://doi.org/10.1021/nm204198g); pmid: [22196055](https://pubmed.ncbi.nlm.nih.gov/22196055/)

## ACKNOWLEDGMENTS

We thank M. Prato for useful discussions. We acknowledge funding from European Union (EU) Graphene Flagship (contract 604391); Newton International Fellowship; faculty start-up support from the University of Texas–Austin; the Welch Foundation Award F-1861; European Research Council grant Hetero2D; a Royal Society Wolfson Research Merit Award, EU projects GENIUS, CARERAMM, and MEM4WIN; Engineering and Physical Sciences Research Council grants EP/K01711X/1, EP/K017144/1, and EP/L016087/1; and Lancaster University’s Distinguished Visitor Program in Physical Sciences.

10.1126/science.1246501



## Graphene, related two-dimensional crystals, and hybrid systems for energy conversion and storage

Francesco Bonaccorso *et al.*

*Science* **347**, (2015);

DOI: 10.1126/science.1246501

*This copy is for your personal, non-commercial use only.*

**If you wish to distribute this article to others**, you can order high-quality copies for your colleagues, clients, or customers by [clicking here](#).

**Permission to republish or repurpose articles or portions of articles** can be obtained by following the guidelines [here](#).

**The following resources related to this article are available online at [www.sciencemag.org](http://www.sciencemag.org) (this information is current as of January 6, 2015):**

**Updated information and services**, including high-resolution figures, can be found in the online version of this article at:

<http://www.sciencemag.org/content/347/6217/1246501.full.html>

This article **cites 128 articles**, 15 of which can be accessed free:

<http://www.sciencemag.org/content/347/6217/1246501.full.html#ref-list-1>

This article appears in the following **subject collections**:

Materials Science

[http://www.sciencemag.org/cgi/collection/mat\\_sci](http://www.sciencemag.org/cgi/collection/mat_sci)